An insight *en-route* from CO_2 fixation to CO_3^{2-}-bridged dinuclear lanthanide(III) complexes featuring inner coordination post-synthetic modification

Vaibhav Singh, Vajeeha Urunikulavan, and Arun Kumar Bar[a]

[a]Indian Institute of Science Education and Research Tirupati, Tirupat-517507, AP, India.
E-mail: a.bar@iisertirupati.ac.in

SUPPORTING INFORMATION
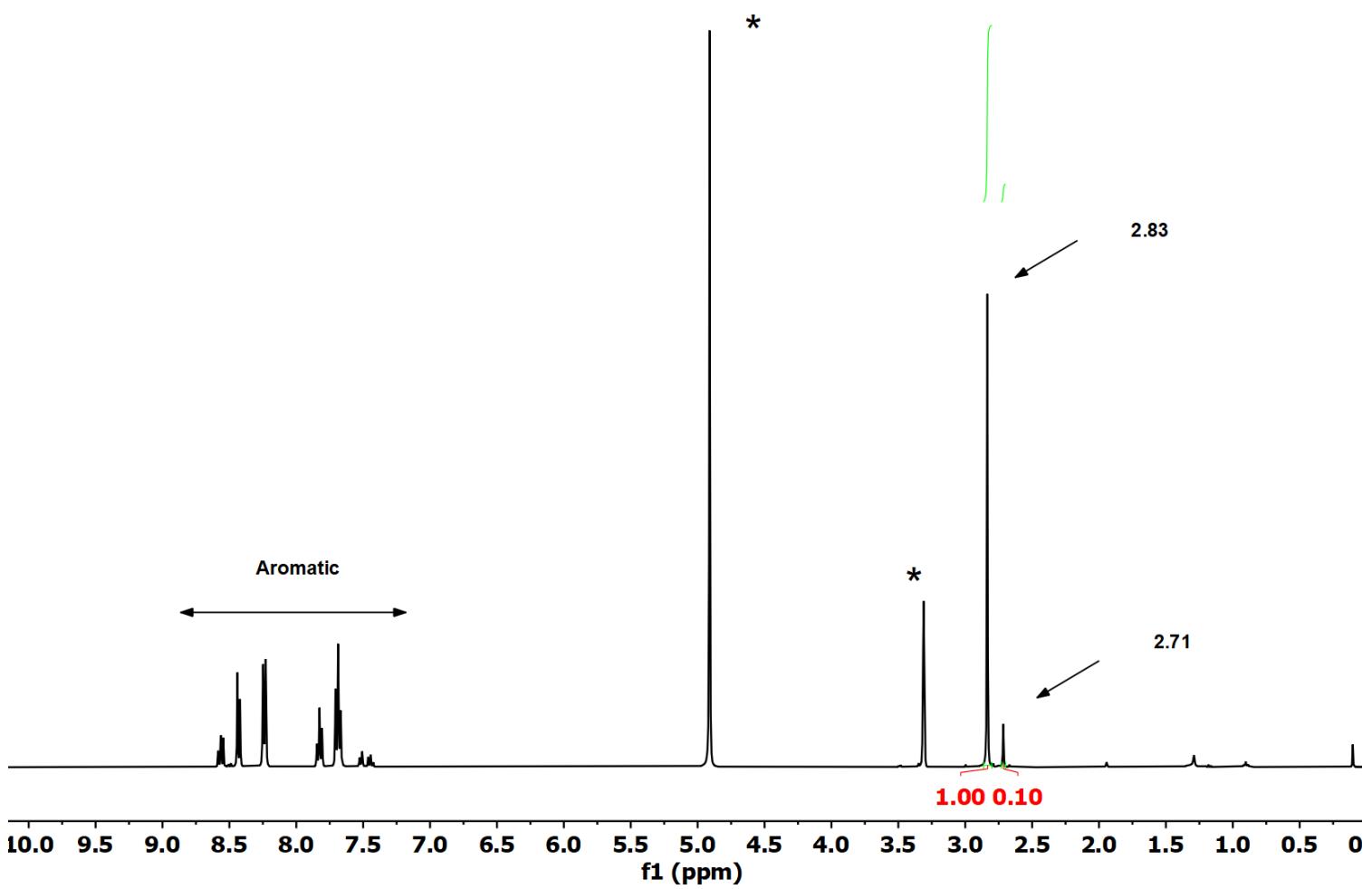
Figure S1: The room temperature solution ^{1}H NMR spectra of the reaction between Y(OTf)$_3$ and H$_2$L in 1:1 equivalency (recorded in CD$_3$OD). The solvent peaks/grease are indicated by asterisks.

[H$_2$LLn (OTf)$_3$] $\rightleftharpoons$ [H$_2$LLn (OTf)$_2$(solvent)] (OTf)

$\uparrow\downarrow$

[H$_2$LLn (OTf)(solvent)$_2$] (OTf)$_2$

$\uparrow\downarrow$

[H$_2$LLn(solvent)$_3$] (OTf)$_3$
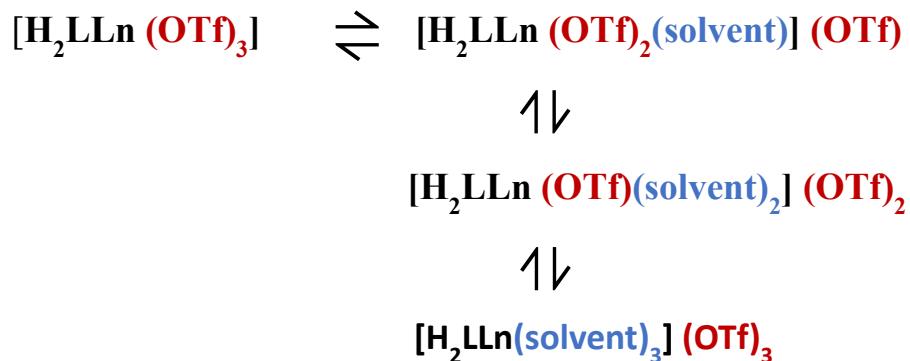
**Scheme S1:** The possible products resulting from the reaction between H$_2$L and Y(OTf)$_3$ in a 1:1 equivalency.
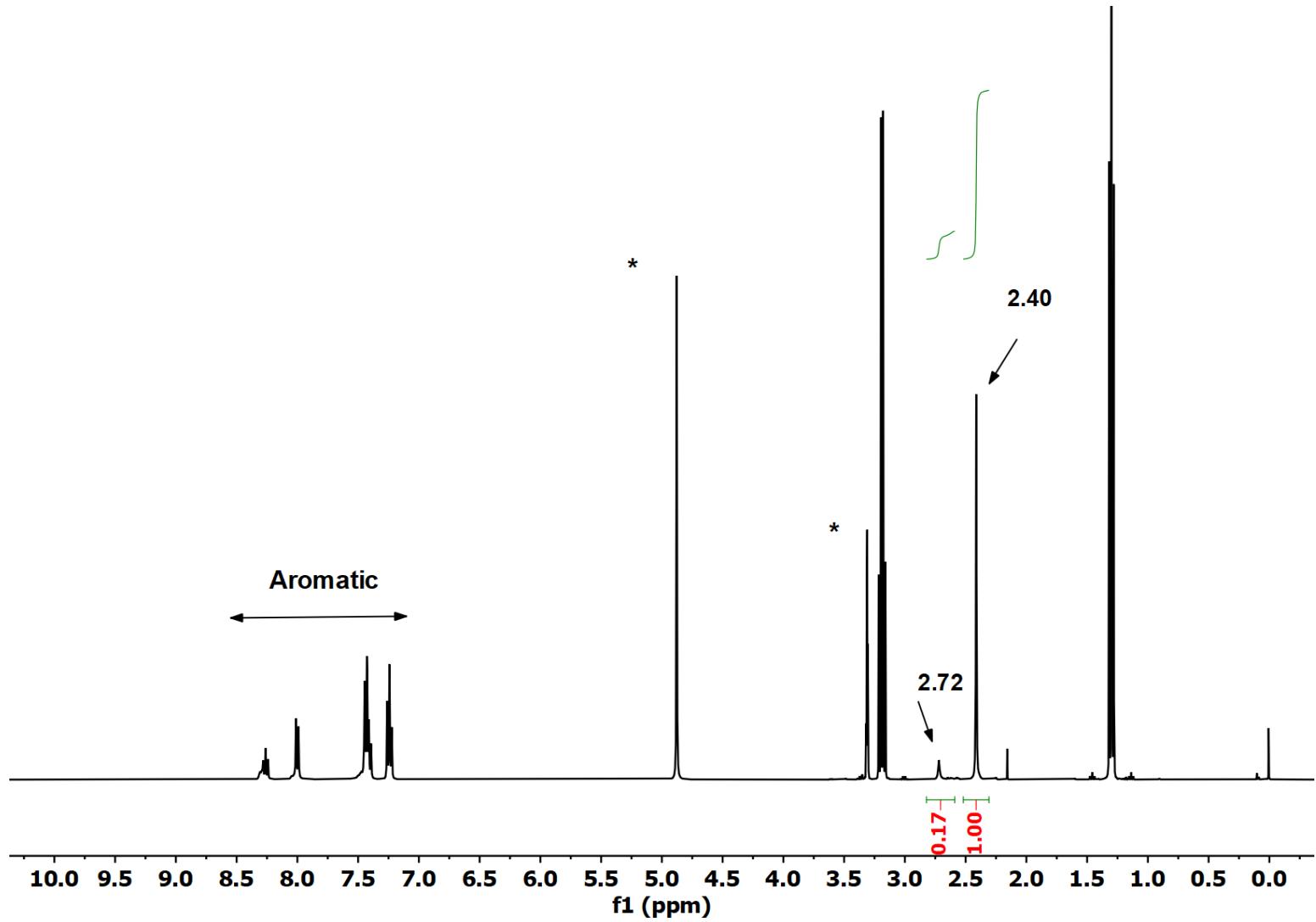
Figure S2: The room temperature solution ^{1}H NMR spectra of the reaction between $Y(OTf)_3$ H_2L and NEt_3 in 1:1:2 equivalency(recorded in CD_3OD). The solvent peaks/grease are indicated by asterisks.
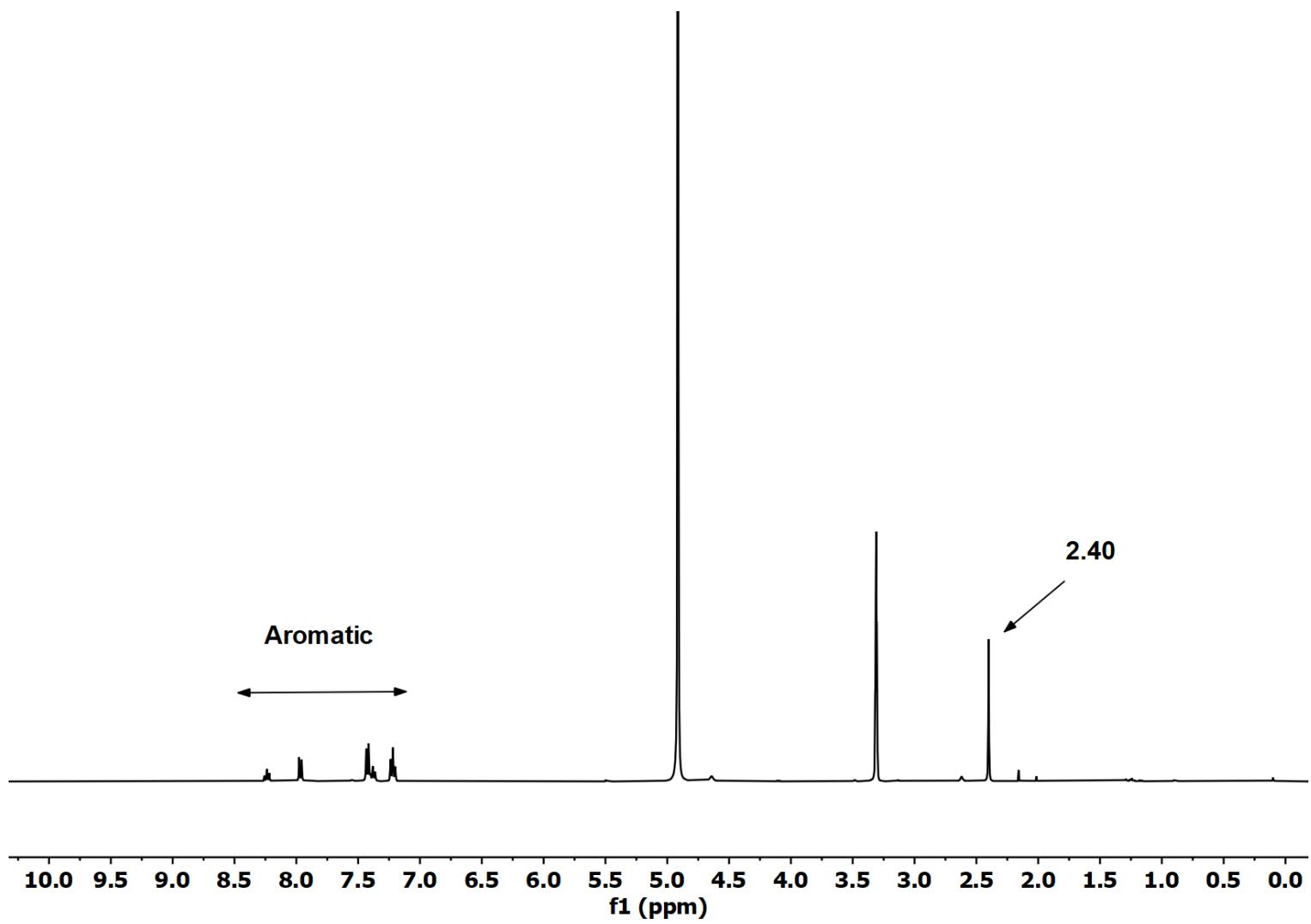
Figure S3: The room temperature solution ^{1}H NMR spectra of the isolated crystals of **4·Y in** CD$_3$OD. The solvent peaks/grease are indicated by asterisks
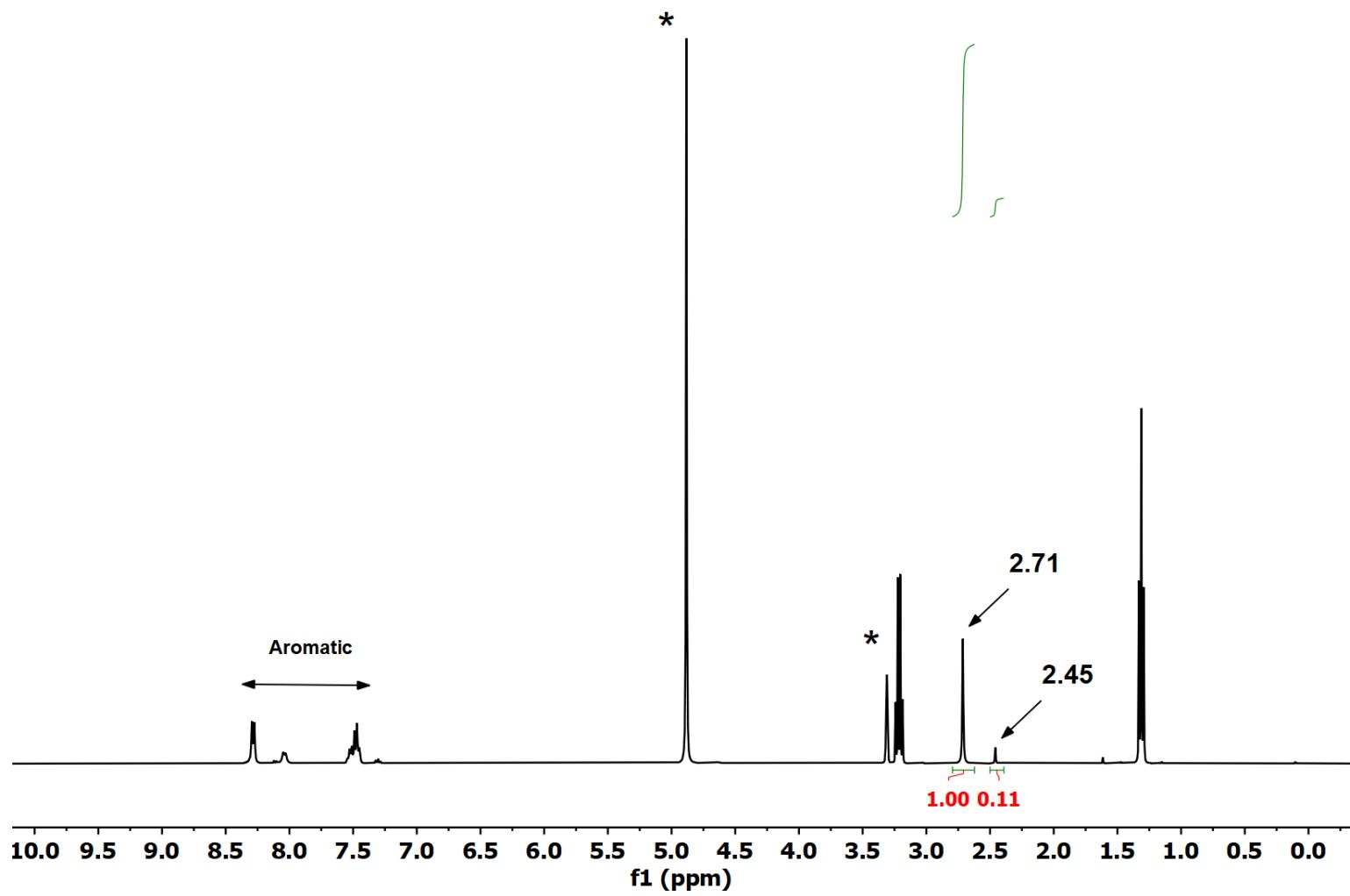
**Figure S4:** The room temperature solution ^{1}H NMR spectra of the reaction between $Y(OTf)_3$, H_2L and NEt_3 in 1:1:2 equivalency, followed by purging of CO_2 gas (recorded in CD_3OD). The solvent peaks/grease are indicated by asterisks.
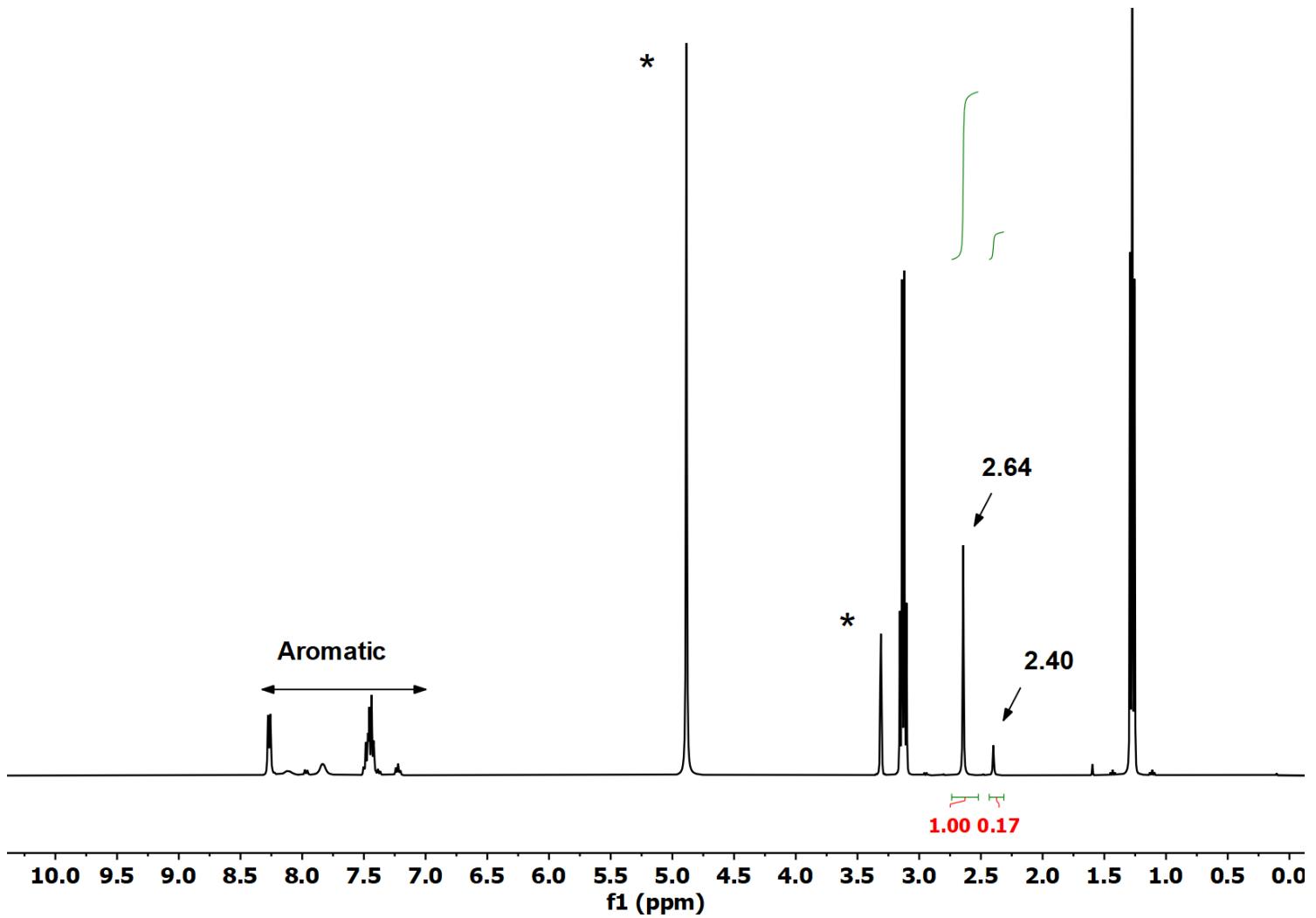
Figure S5: The room temperature solution ^1H NMR spectra of the reaction between Y(OTf)$_3$, H$_2$L and NEt$_3$ in 1:1:3 equivalency, followed by purging of CO$_2$ gas (recorded in CD$_3$OD). The solvent peaks/grease are indicated by asterisks.
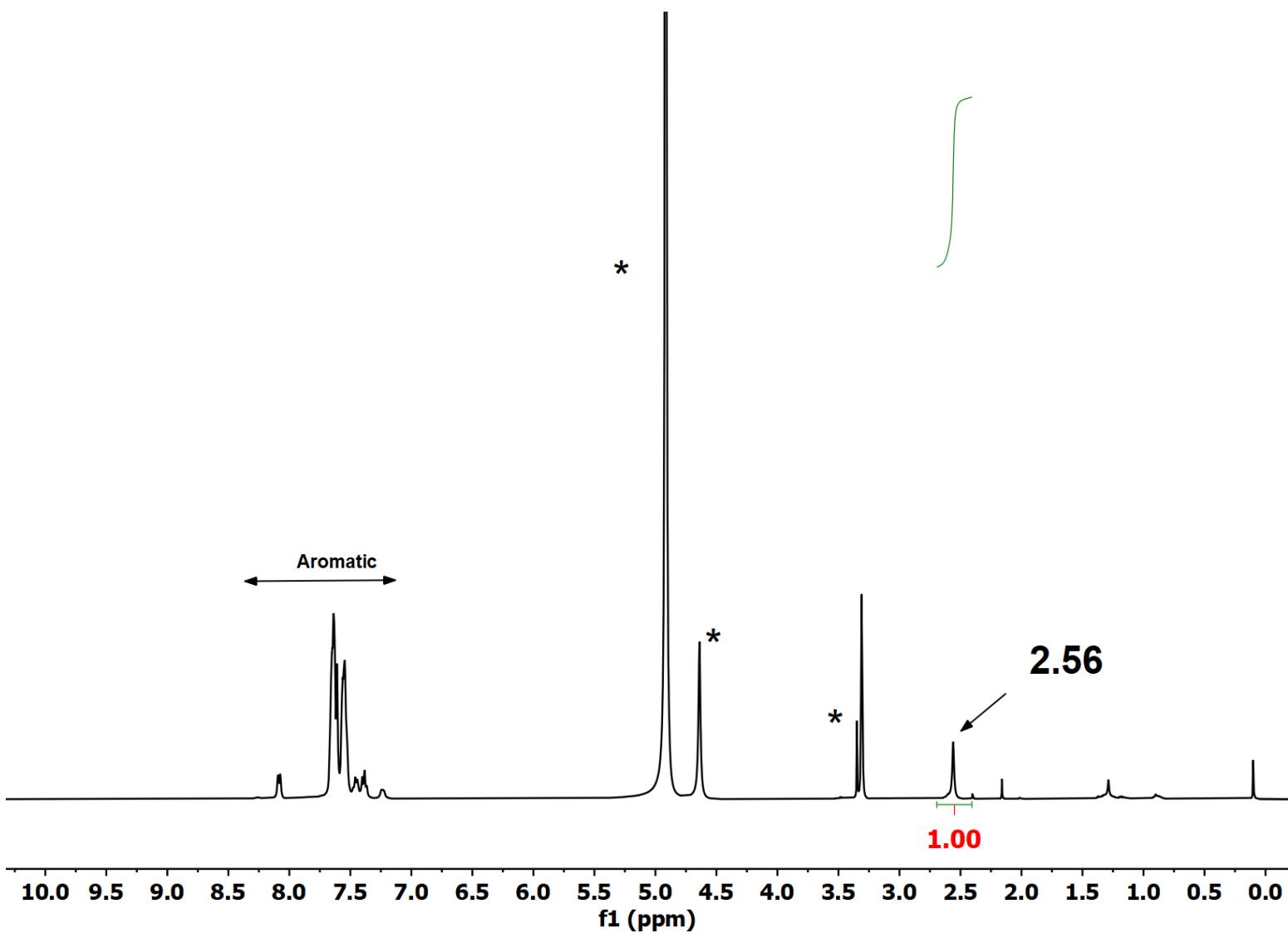
Figure S6: The room temperature solution ^1H NMR spectra of the reaction between gelatinous ppt. and CO_2 gas followed by addition of 2eq of TPPO (recorded in CD_3OD). The solvent peaks/grease are indicated by asterisks.
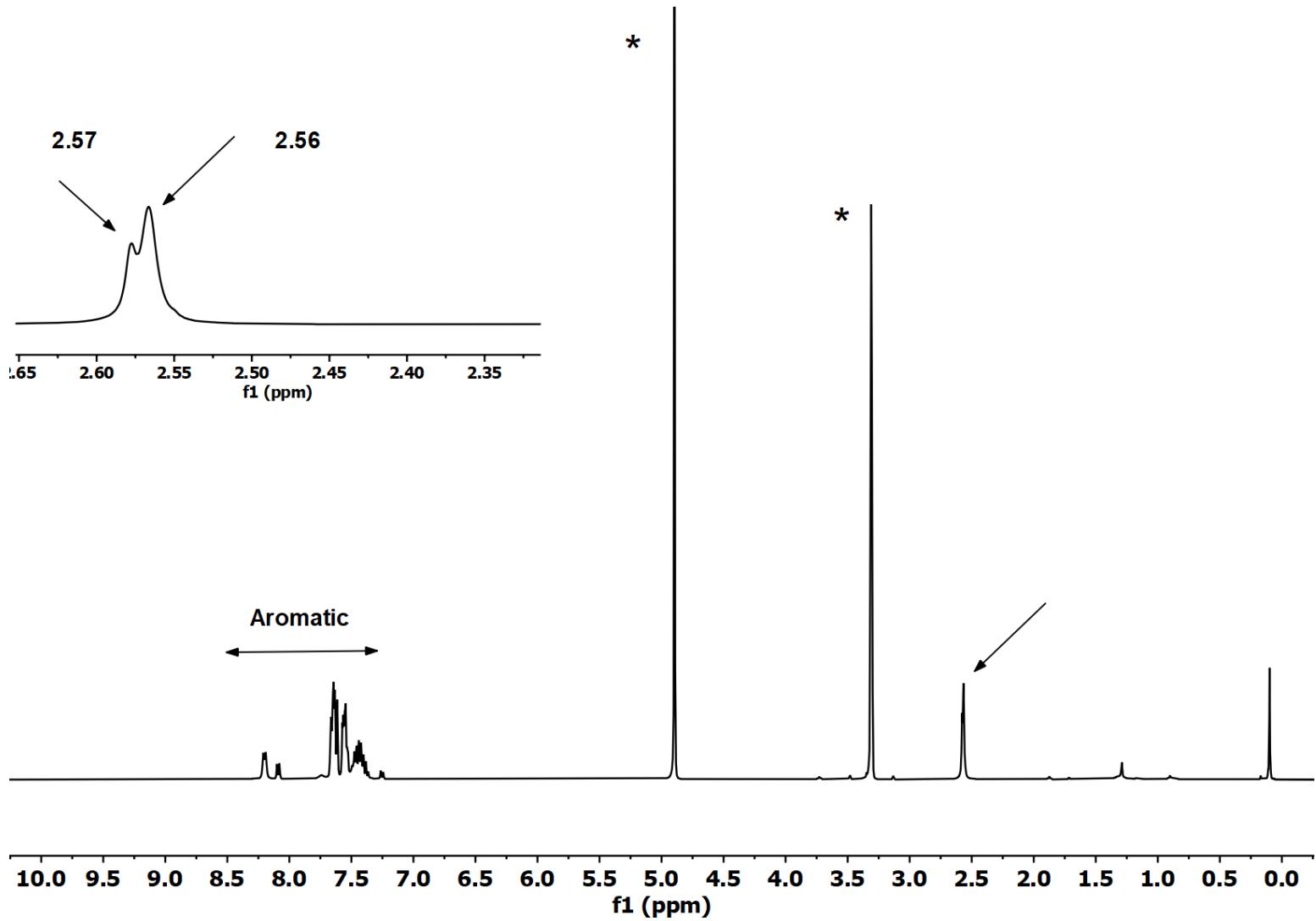
Figure S7: NMR signal for the doubly substituted phosphine oxide (2.56 ppm) analogues equilibrating with corresponding singly substituted phosphine oxide congeners (2.57 ppm). The solvent peaks/grease are indicated by asterisks.
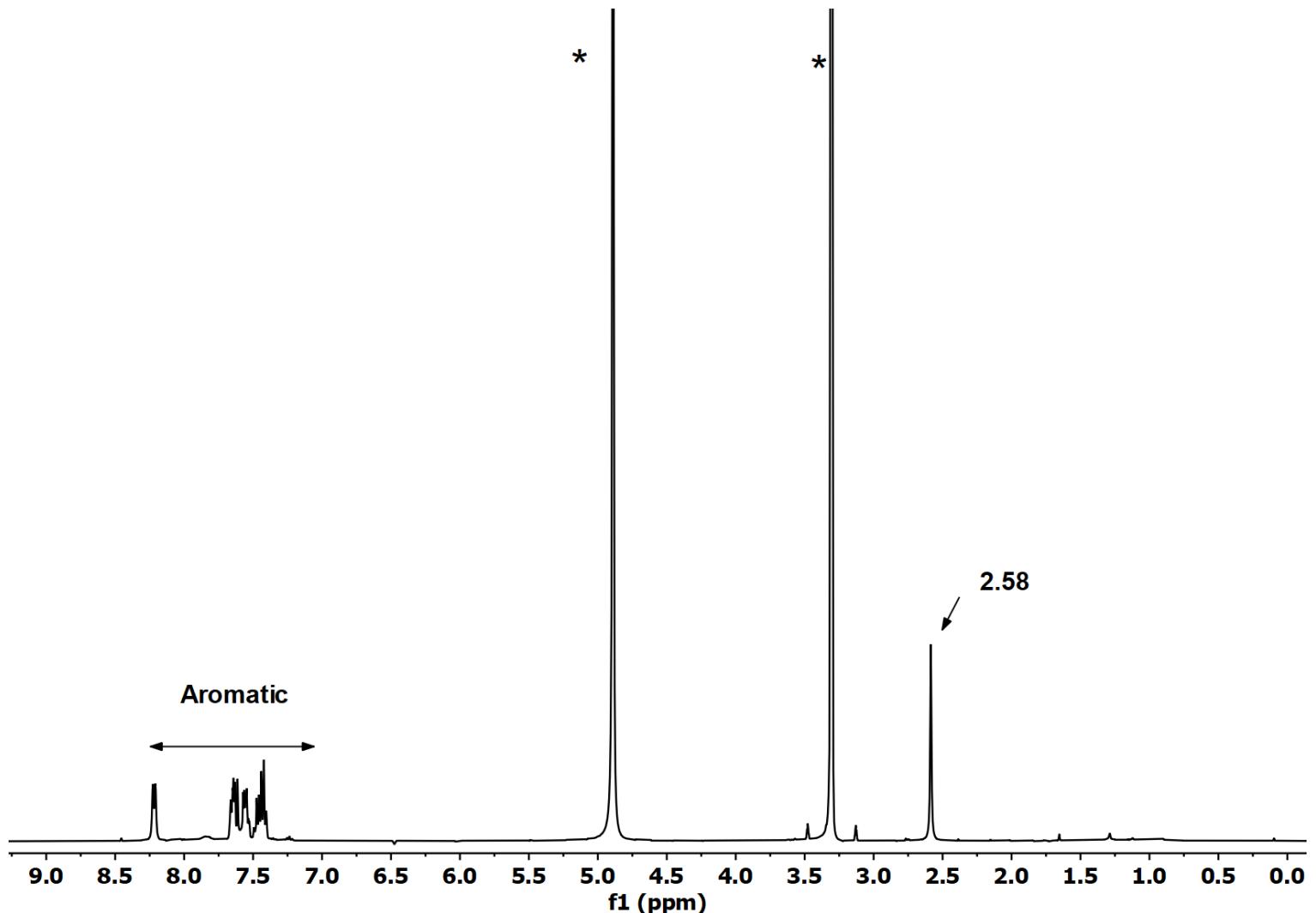
Figure S8: The room temperature solution ^{1}H NMR spectra of the isolated crystals of **5·Y in** CD$_3$OD. The solvent peaks/grease are indicated by asterisks
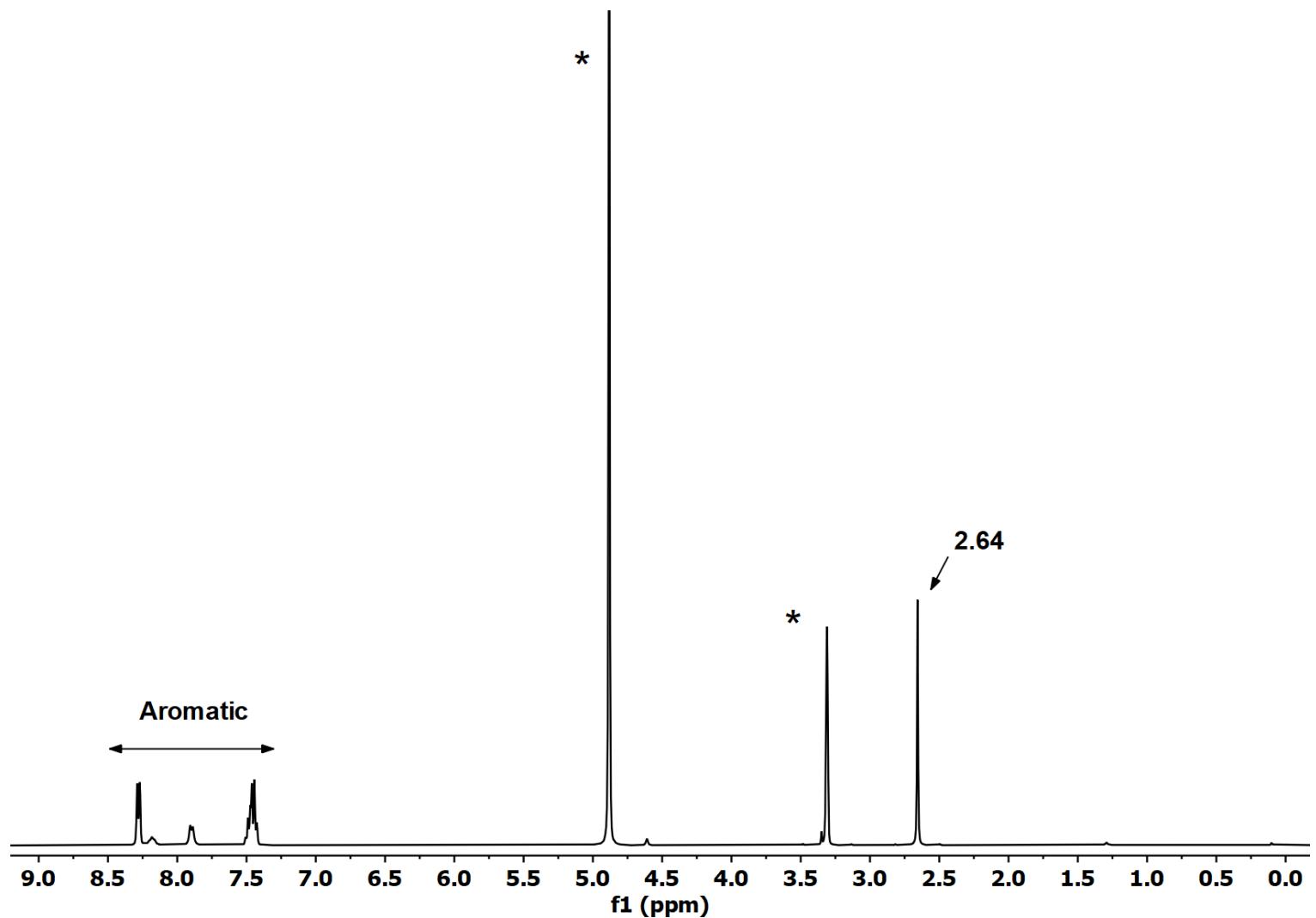
Figure S9: The room temperature solution ^{1}H NMR spectra of the isolated crystals of **2·Y in** CD$_3$OD. The solvent peaks/grease are indicated by asterisks
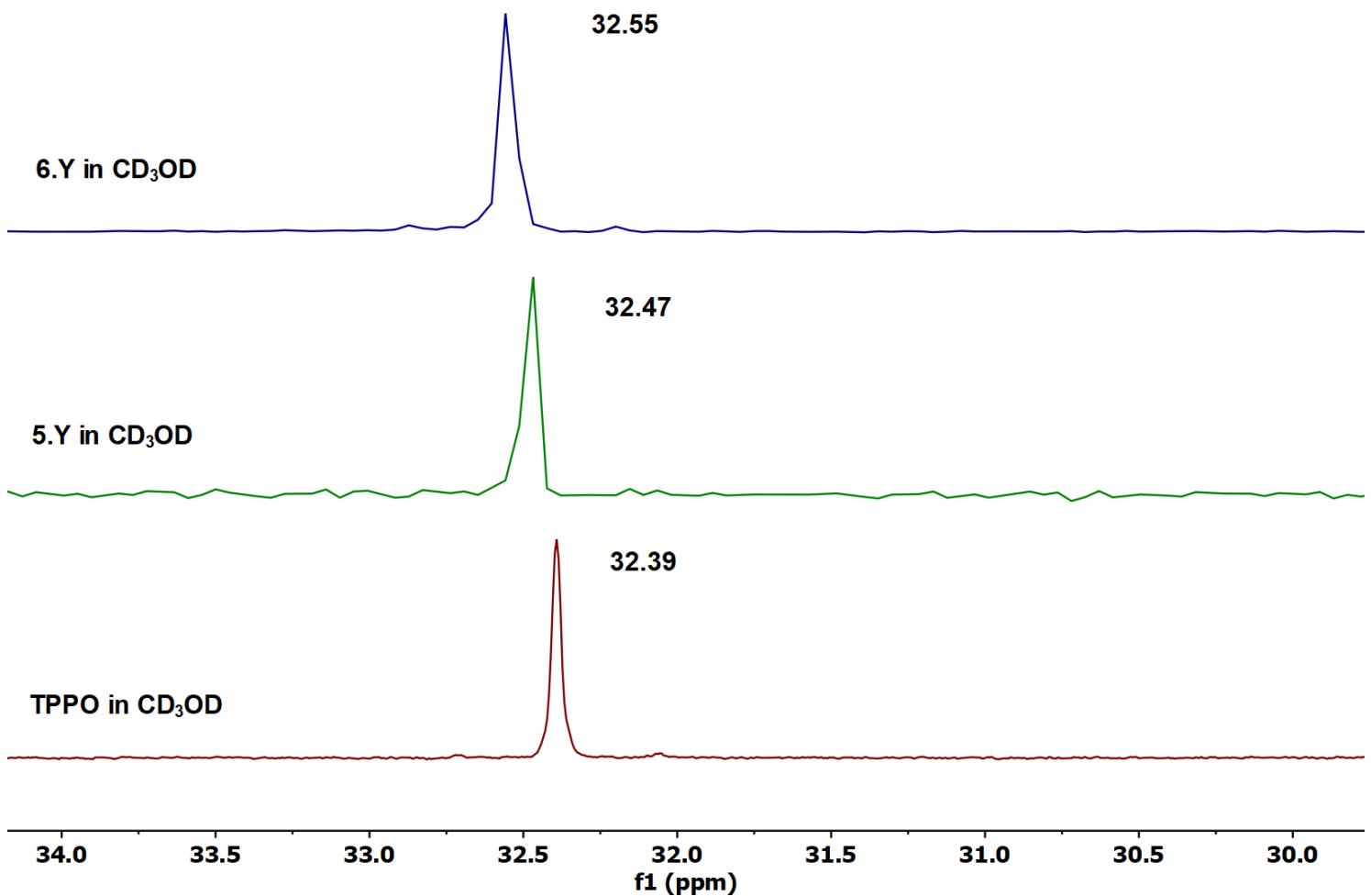
Figure S10: The comparative ^{31}P NMR spectra of TPPO (red), **5·Y**(green), and **6·Y**(blue) recorded in CD$_3$OD solution at room temperature.
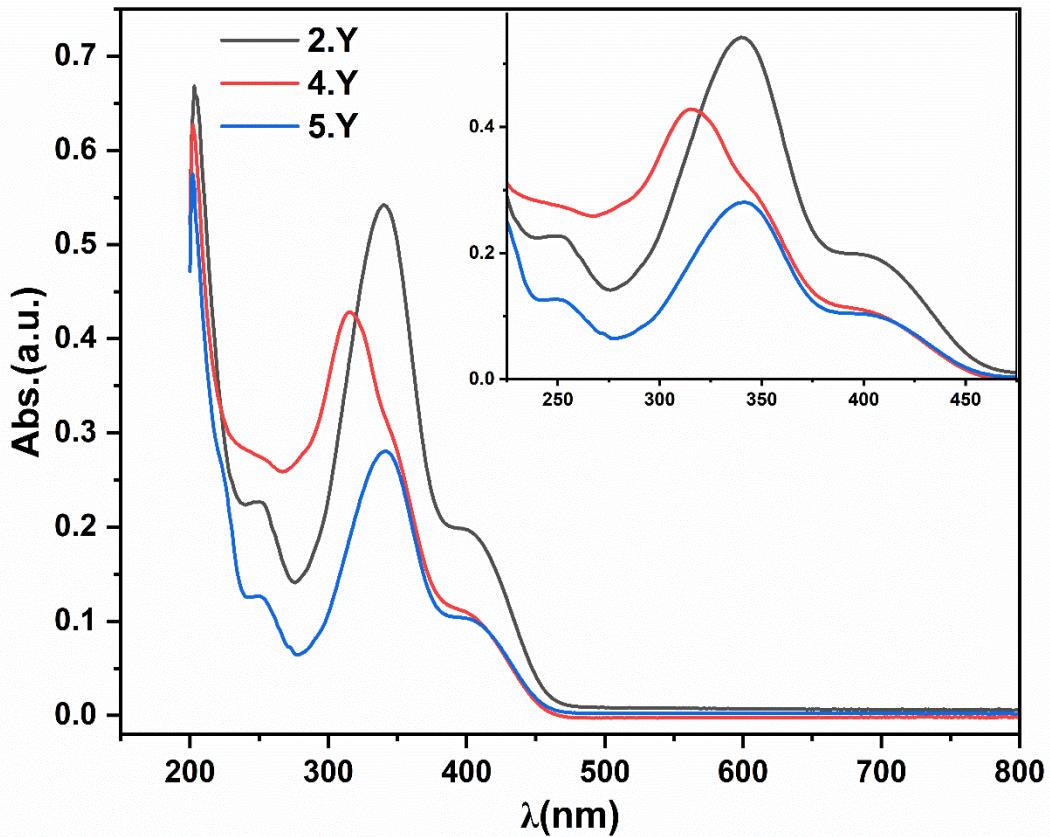
Figure S11: The comparative UV-Vis absorption spectra of the methanolic solutions (10μM) of **2·Y** (black), **4·Y** (red), and **5·Y** (blue), recorded at room temperature. The insets are the zoomed-in absorptions in the 225-475 nm regions.

Table S1: The absorption maxima(λ_{max}^{abs})and the corresponding molar extinction coefficients for the as-synthesized complexes in MeOH under ambient conditions.

	λ_{max}^{abs}(nm)				ε(M^{-1}cm^{-1})			
2·Y	392	340	250	203	20000	54200	22600	67000
5·Y	392	342	249	202	11000	28000	12700	57400
4·Y	392	315		202	11300	42800		62700
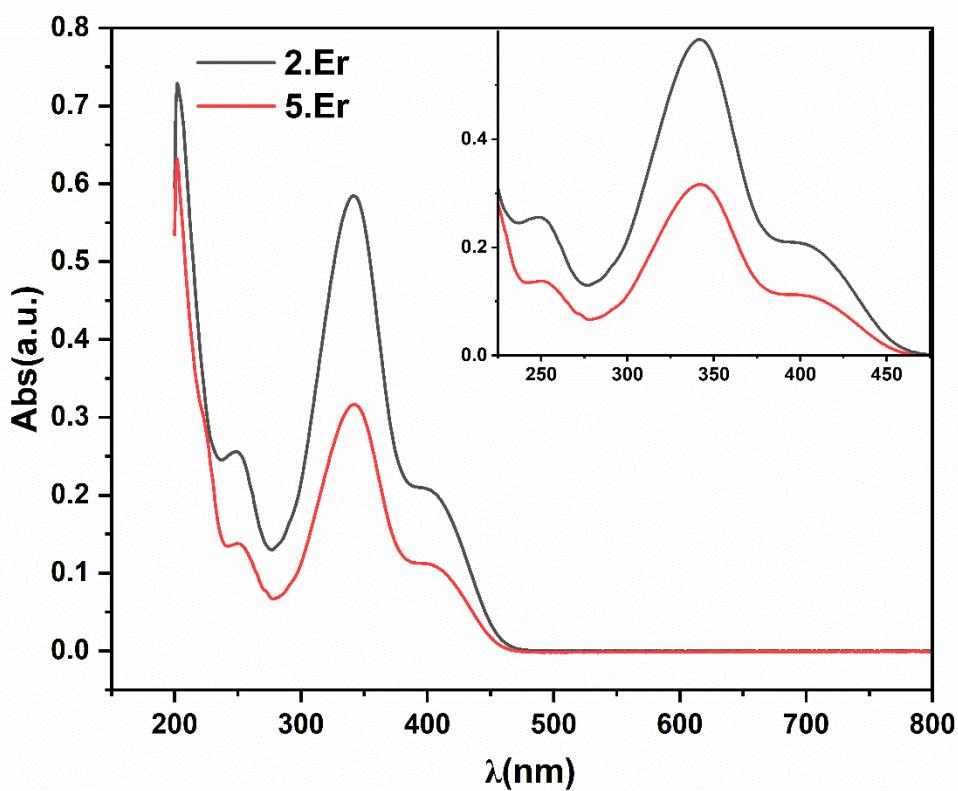
Figure S12: The comparative UV-Vis absorption spectra of the methanolic solutions (10μM) of **2·Er** (black), and **5·Er** (red), recorded at room temperature. The insets are the zoomed-in absorptions in the 225-475 nm regions

Table S2: The absorption maxima(λ_{max}^{abs})and the corresponding molar extinction coefficients for the as-synthesized complexes in MeOH under ambient conditions.

	$\lambda_{max}^{abs}(nm)$				$\varepsilon(M^{-1}cm^{-1})$			
2·Er	*392*	*341*	*249*	*203*	*21000*	*58000*	*26000*	*72300*
5·Er	*392*	*342*	*250*	*202*	*11200*	*31600*	*13800*	*61300*
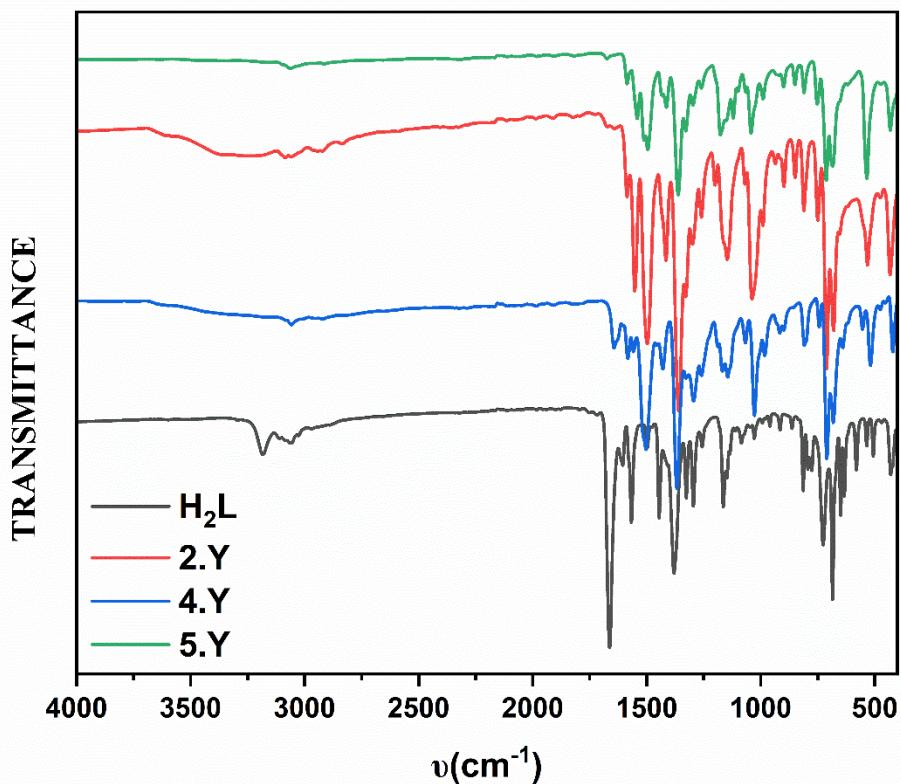
Figure S13. Comparative solid-state FT-IR spectra of the Schiff base ligands **H₂L** (black) and the Y analogues **2·Y** (red), **4·Y**(blue) and **5·Y** (green) recorded at room temperature.

Table S3: The characteristic stretching frequencies corresponding to the C=O and C=N functional groups in the Schiff base ligand and in the complexes. The assignment of the stretching frequencies is based on the reported literature.

| Compound	$U_{C=O}(cm^{-1})$	$U_{C=N}(cm^{-1})$
H₂L	1662(vs),1605(m)	1567(s)
2·Y	1552(s)	1640(w),1586(m)
4·Y	1558(m)	1644(w),1582(m)
5·Y	1542(m)	1670(w),1586(m)
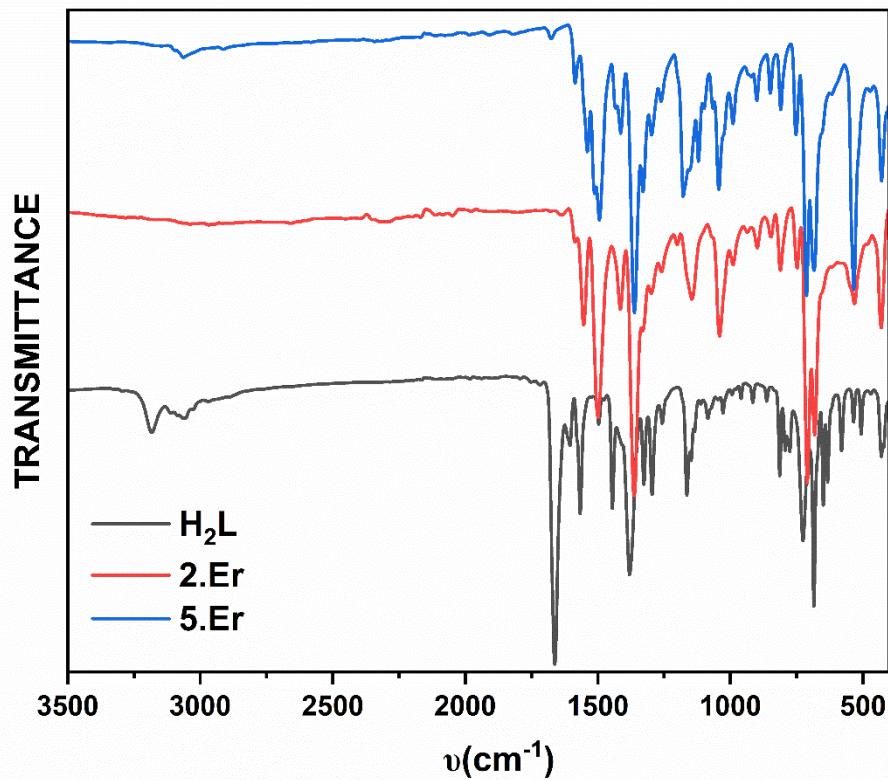
Figure S14. Comparative solid-state FT-IR spectra of the Schiff base ligands **H₂L** (black) and the Er analogues **2·Er** (red) and **5·Er**(blue) recorded at room temperature.

Table S4: The characteristic stretching frequencies corresponding to the C=O and C=N functional groups in the Schiff base ligand and in the complexes. The assignment of the stretching frequencies is based on the reported literature.

Compound	$U_{C=0}(cm^{-1})$	$U_{C=N}(cm^{-1})$
H₂L	1662(vs),1605(m)	1567(s)
2·Er	1554(s)	1634(w),1586(m)
5·Er	1540(m)	1670(w),1586(m)
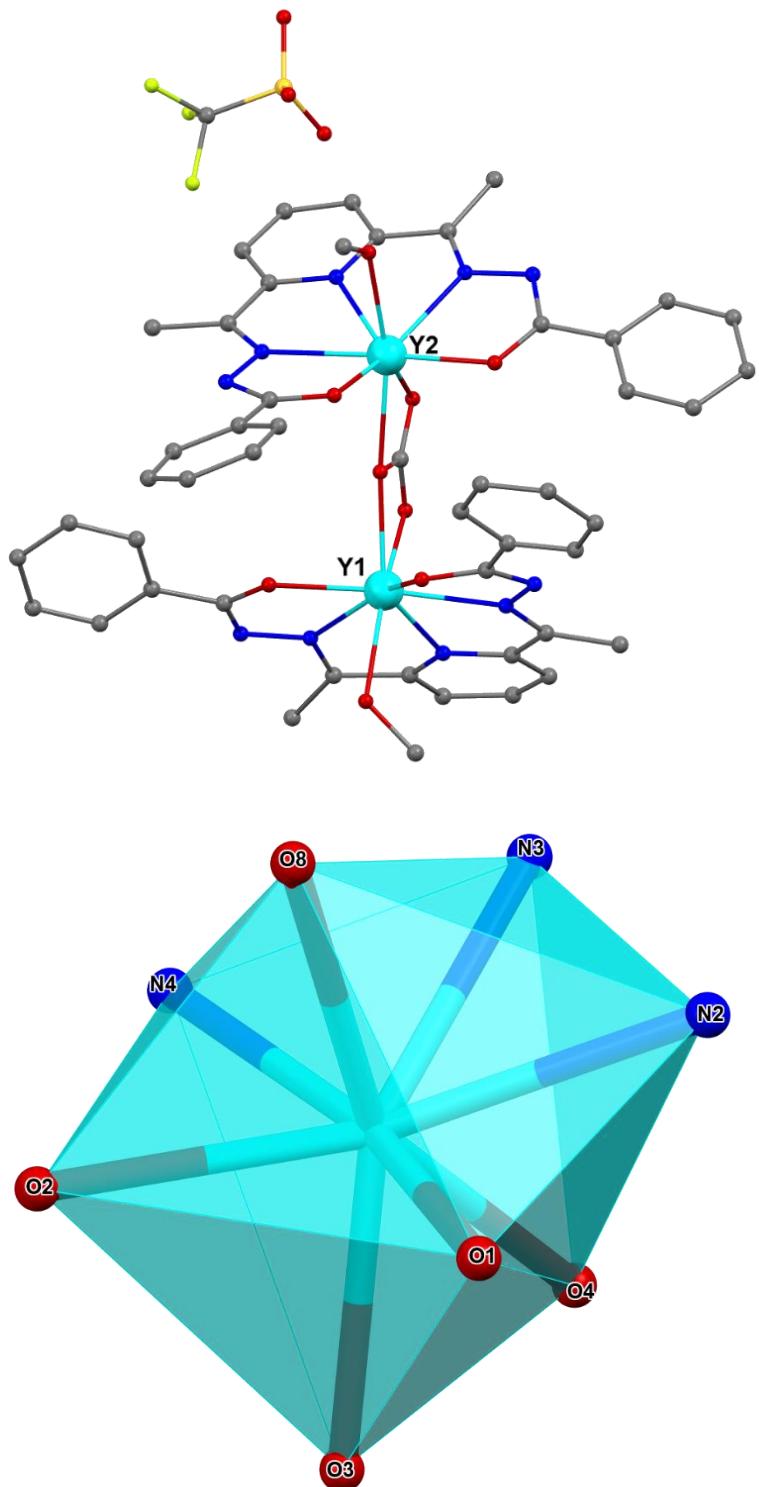
Figure S15*: Top: The ball-and-stick models for the asymmetric unit of the single-crystal X-ray molecular structures of the **1·Y .**H atoms and co-crystallised solvents in **1·Y** are omitted for clarity. Colour codes: cyan, Y; red, O; blue, N; grey, C; green, F; yellow, S. **Bottom*:** The coordination polyhedron around the Y centre of **1·Y**.
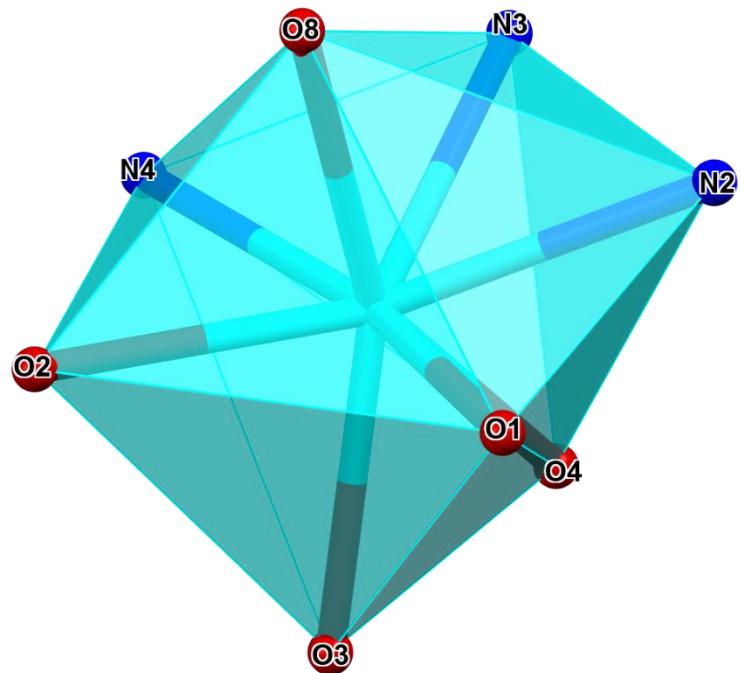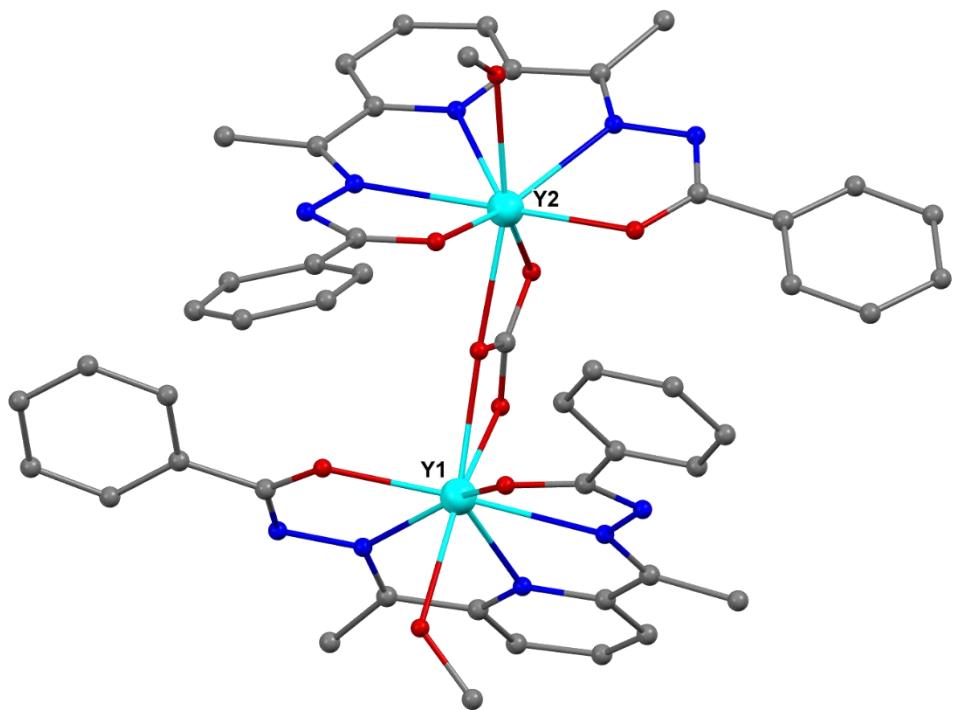
Figure S16: **Top:** The ball-and-stick models for the asymmetric unit of the single-crystal X-ray molecular structures of the **2·Y**. H atoms and co-crystallised solvents in **2·Y** are omitted for clarity. Colour codes: cyan, Y; red, O; blue, N; grey, C. **Bottom:** The coordination polyhedron around the Y centre of **2·Y**.
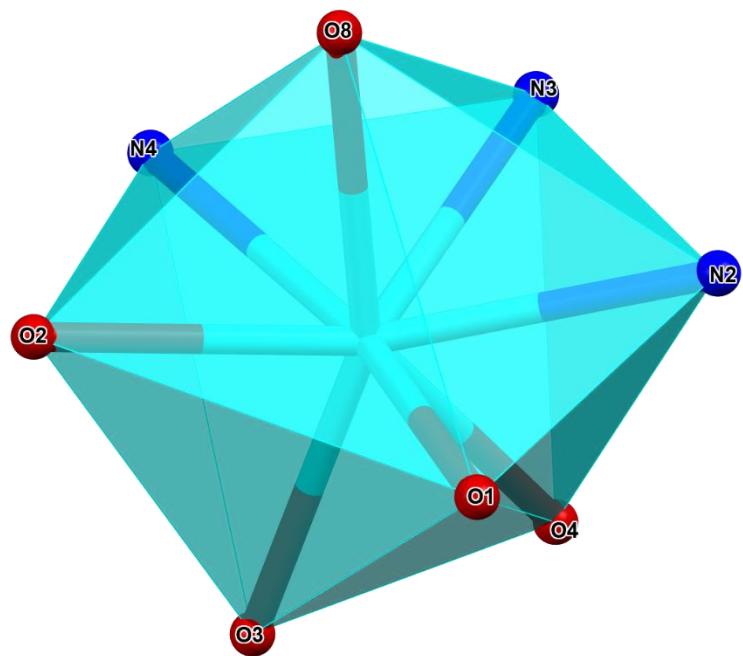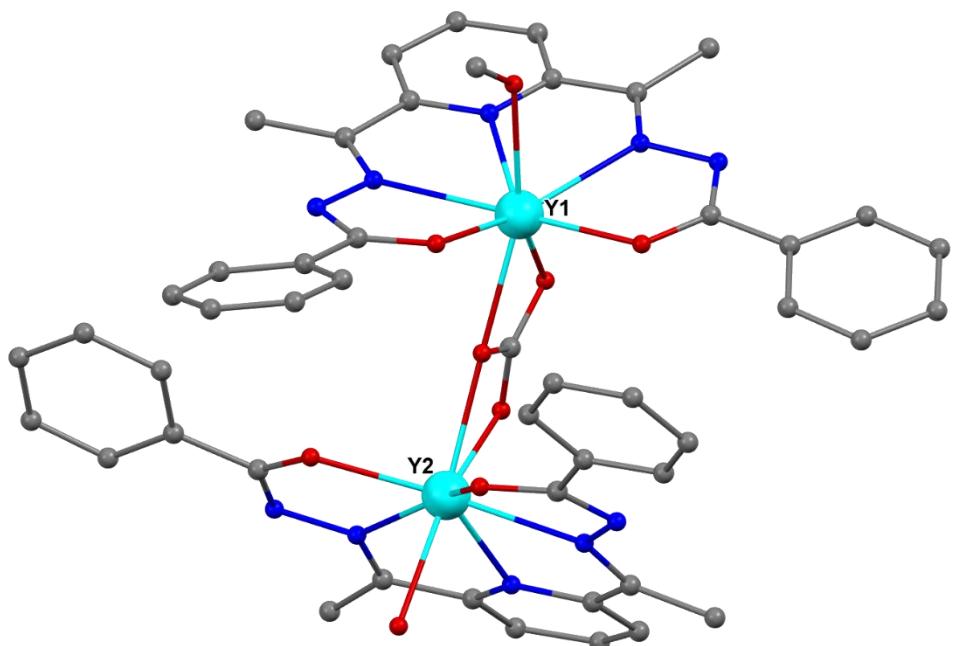
Figure S17: **Top:** The ball-and-stick models for the asymmetric unit of the single-crystal X-ray molecular structures of the **3·Y** .H atoms and co-crystallised solvents in **3·Y** are omitted for clarity. Colour codes: cyan, Y; red, O; blue, N; grey, C. **Bottom:** The coordination polyhedron around the Y centre of **3·Y**.
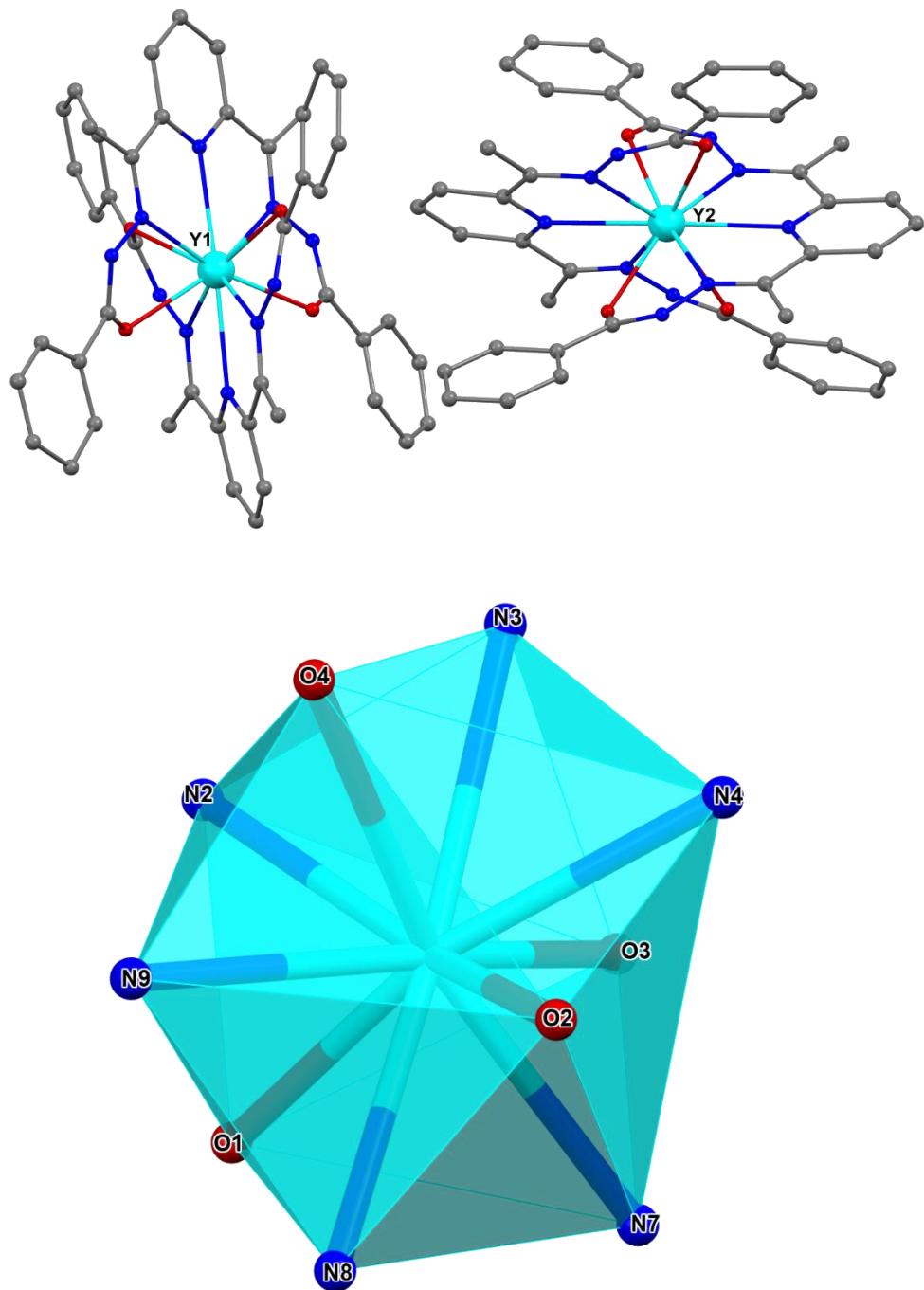
Figure S18*:* **Top:** The ball-and-stick models for the asymmetric unit of the single-crystal X-ray molecular structures of the **4·Y** .H atoms and co-crystallised solvents in **4·Y** are omitted for clarity. Colour codes: cyan, Y; red, O; blue, N; grey, C. **Bottom***:* The coordination polyhedron around the Y centre of **4·Y**
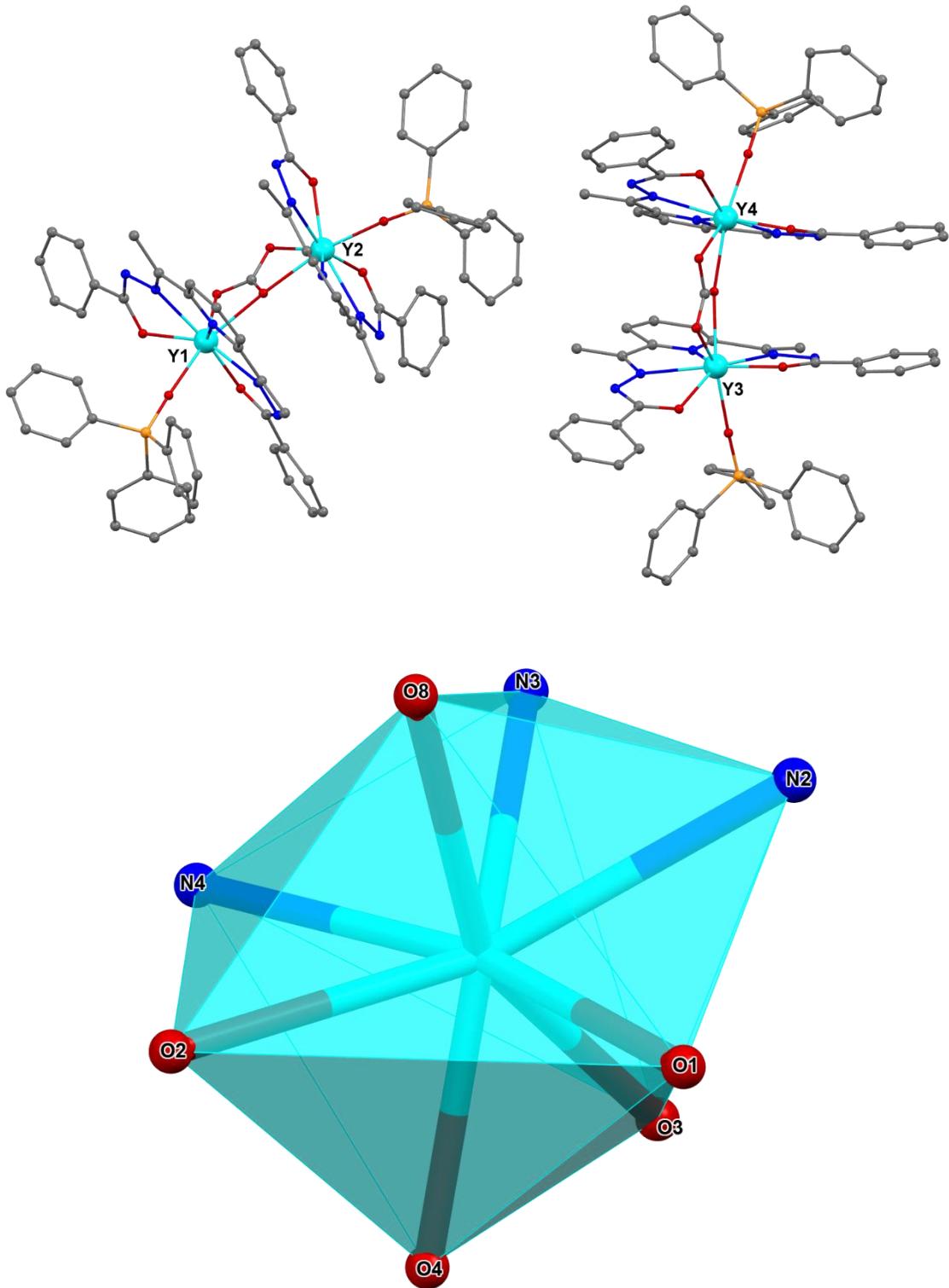
Figure S19*: Top: The ball-and-stick models for the asymmetric unit of the single-crystal X-ray molecular structures of the **6·Y** .H atoms and co-crystallised solvents in **6·Y** are omitted for clarity. Colour codes: cyan, Y; red, O; blue, N; grey, C; orange, P. **Bottom:** The coordination polyhedron around the Y centre of **6·Y**
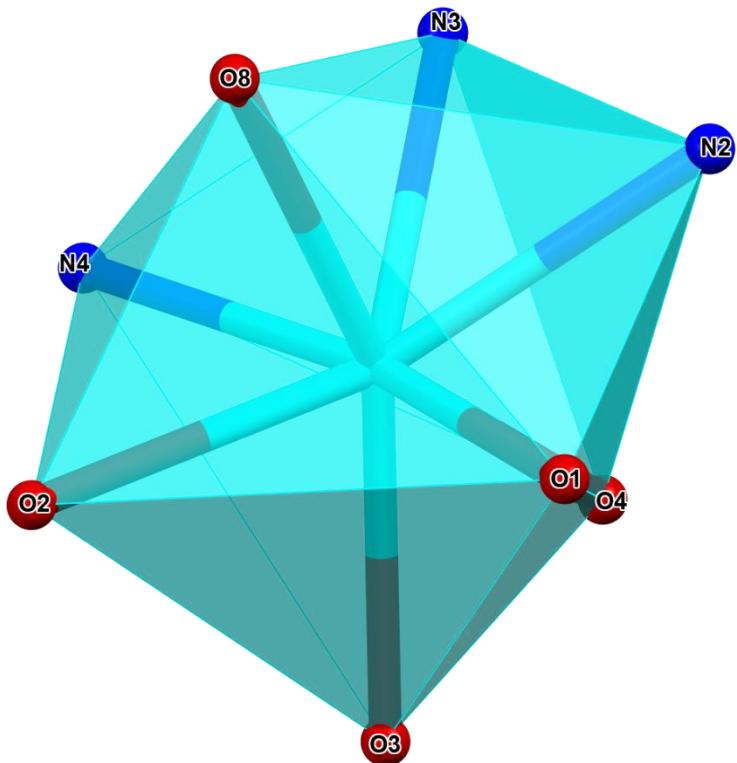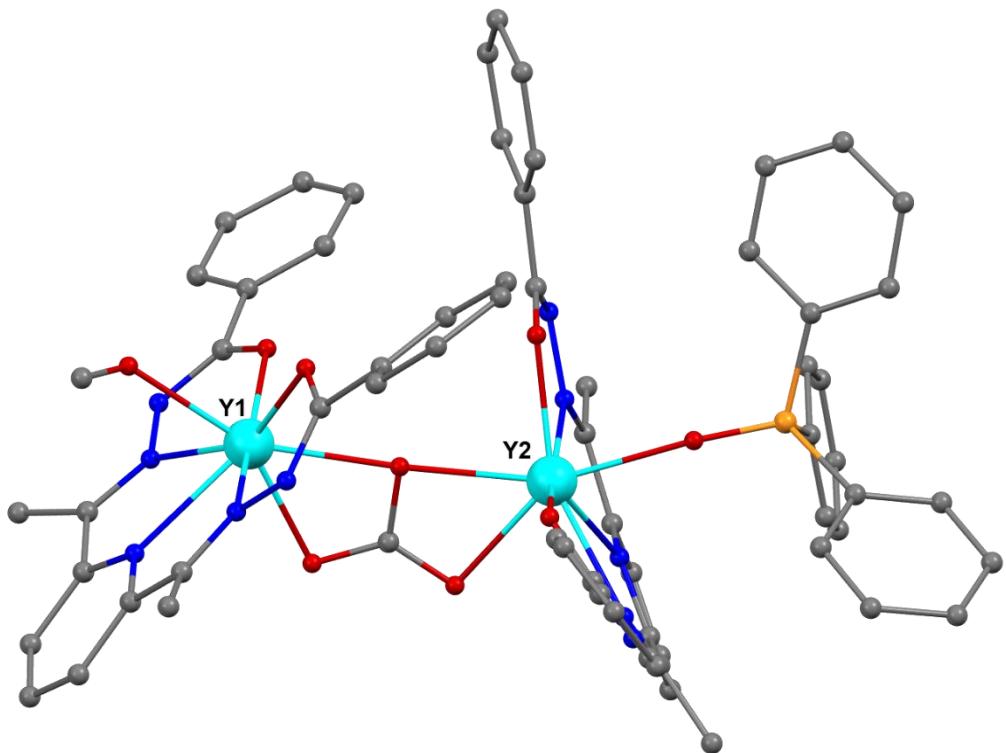
Figure S20*:* **Top:** The ball-and-stick models for the asymmetric unit of the single-crystal X-ray molecular structures of the **5·Y** .H atoms and co-crystallised solvents in **5·Y** are omitted for clarity. Colour codes: cyan, Y; red, O; blue, N; grey, C; orange, P. **Bottom***:* The coordination polyhedron around the Y centre of **5·Y**
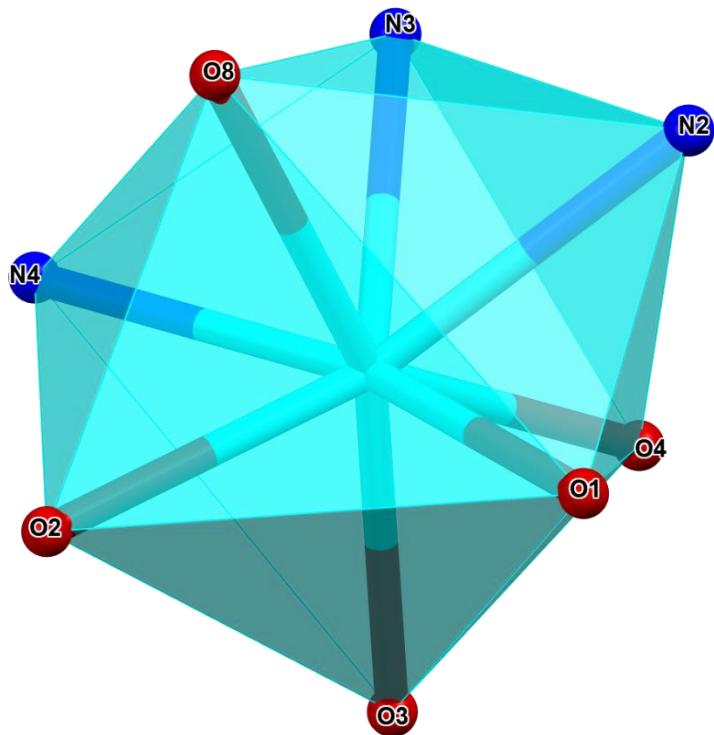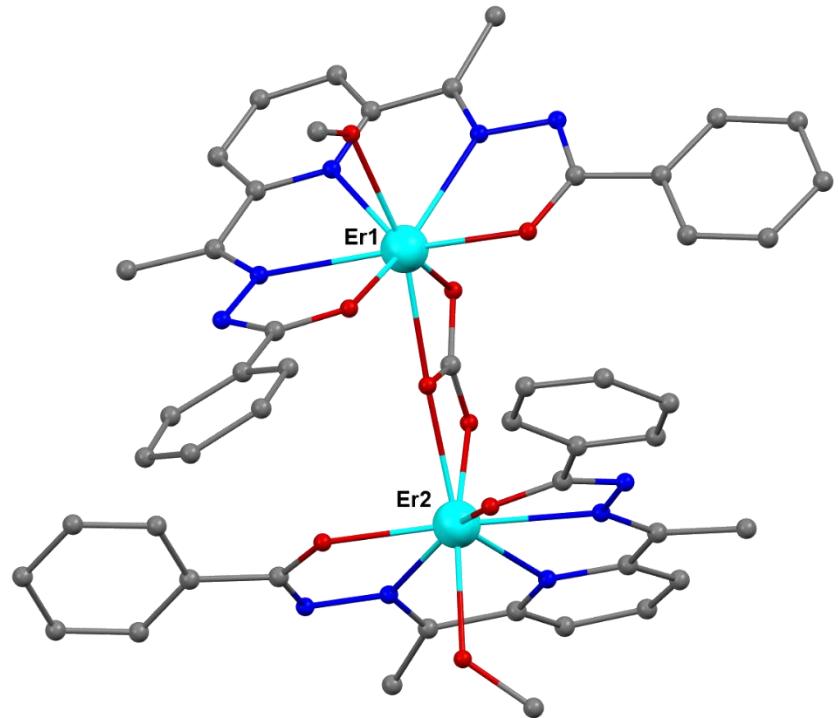
**Figure S21*: Top:** The ball-and-stick models for the asymmetric unit of the single-crystal X-ray molecular structures of the **2·Er .**H atoms and co-crystallised solvents in **2·Er** are omitted for clarity. Colour codes: cyan, Y; red, O; blue, N; grey, C. **Bottom*:** The coordination polyhedron around the Y centre of **2·Er**
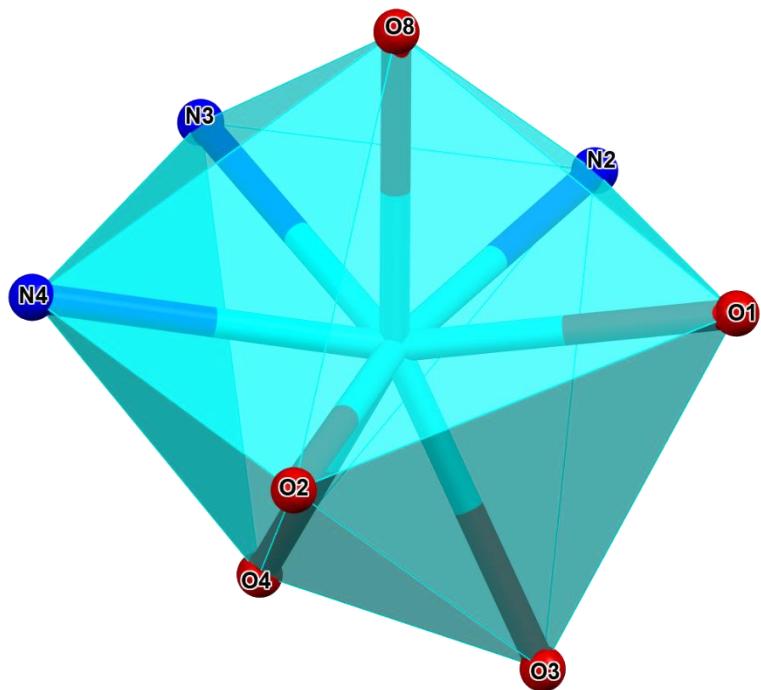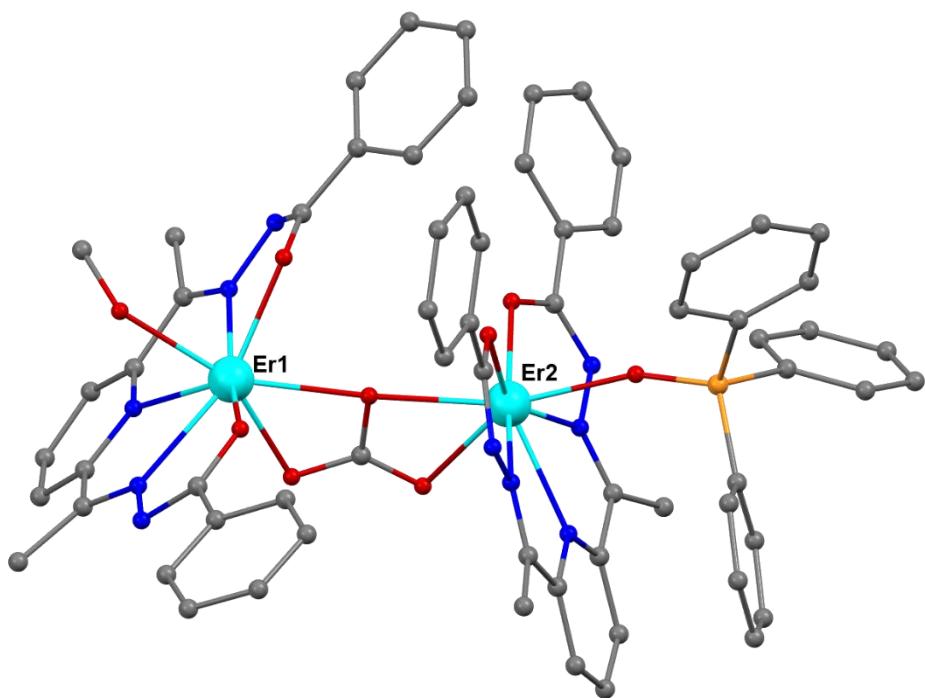
Figure S22*:* Top: The ball-and-stick models for the asymmetric unit of the single-crystal X-ray molecular structures of the **5·Er**.H atoms and co-crystallised solvents in **5·Er** are omitted for clarity. Colour codes: cyan, Y; red, O; blue, N; grey, C; orange, P. **Bottom*:*** The coordination polyhedron around the Y centre of **5·Er**
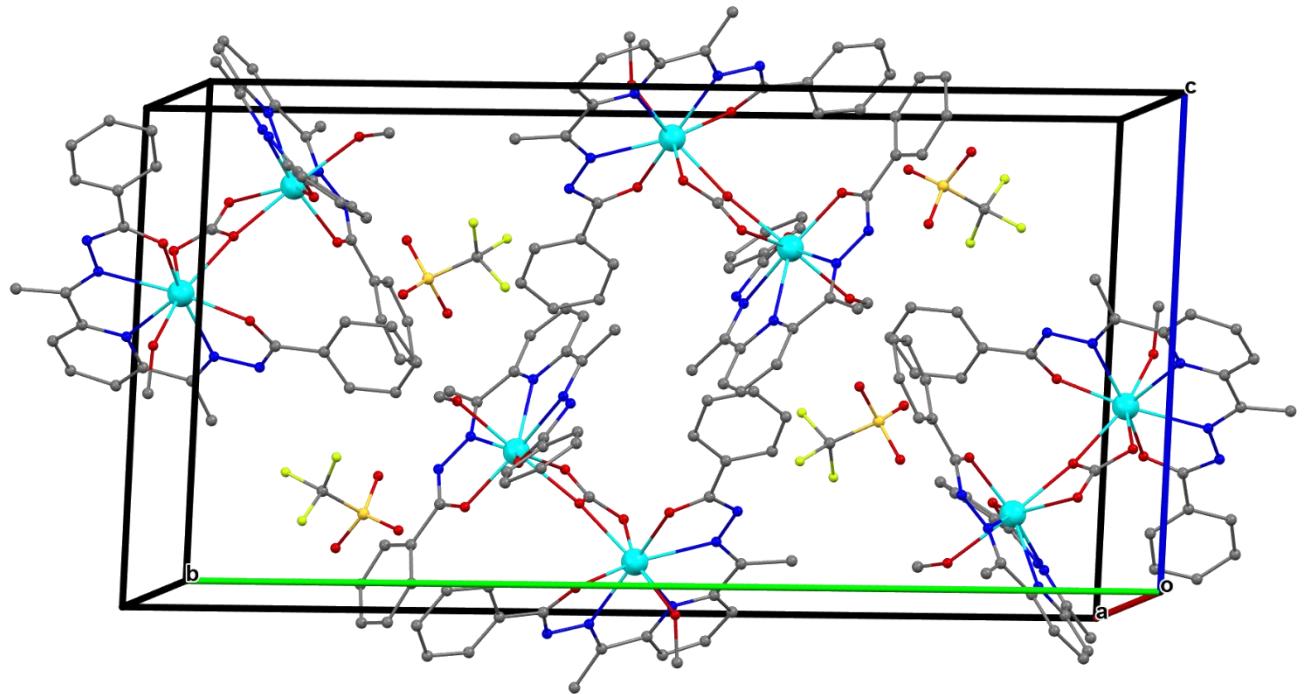
Figure S23: Unit cell contents of **1·Y** . Colour codes: cyan, Y; red, O; blue, N; grey, C; green F; yellow, S.
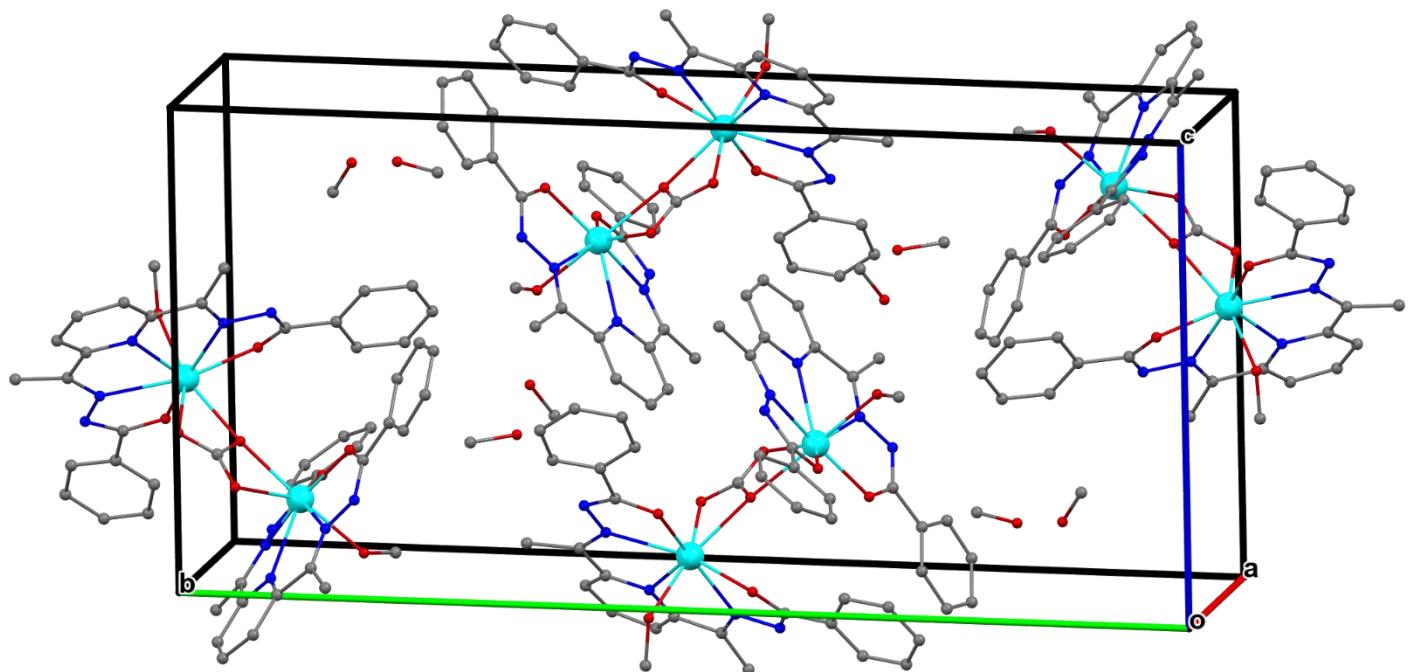
Figure S24: Unit cell contents of **2·Y** . Colour codes: cyan, Y; red, O; blue, N; grey, C.
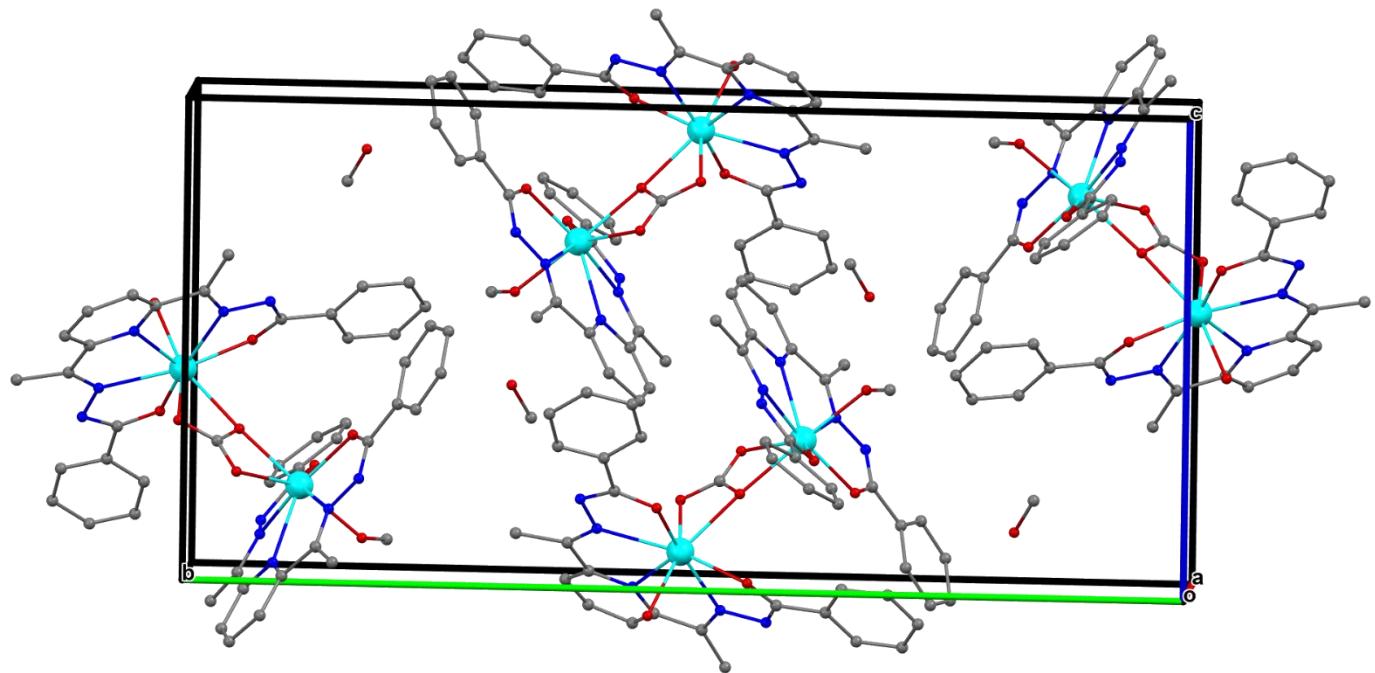
Figure S25: Unit cell contents of **3·Y .** Colour codes: cyan, Y; red, O; blue, N; grey, C.
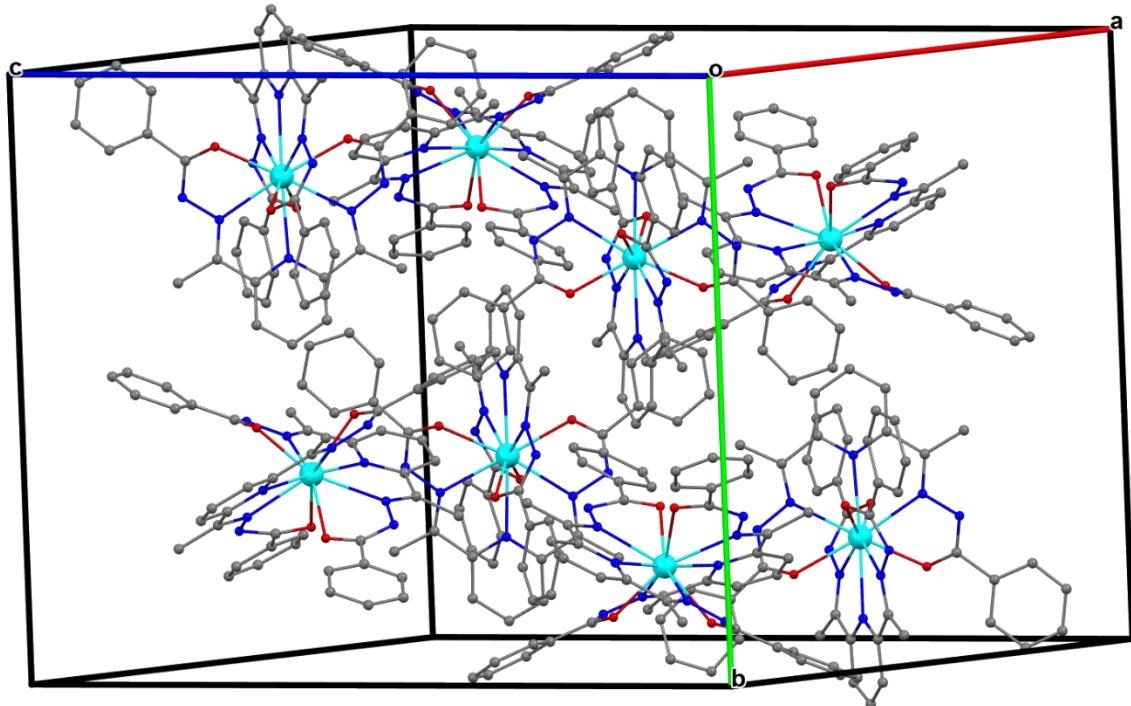
Figure S26: Unit cell contents of **4·Y .** Colour codes: cyan, Y; red, O; blue, N; grey, C
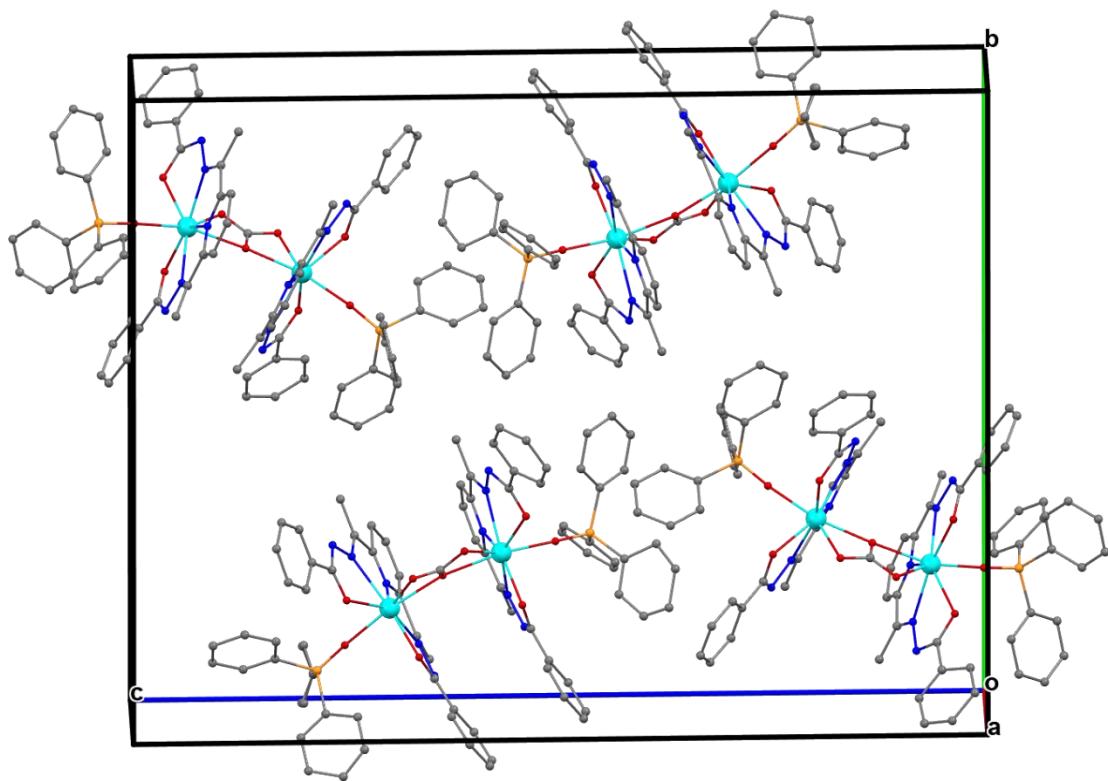
Figure S27: Unit cell contents of **6·Y .** Colour codes: cyan, Y; red, O; blue, N; grey, C; orange, P
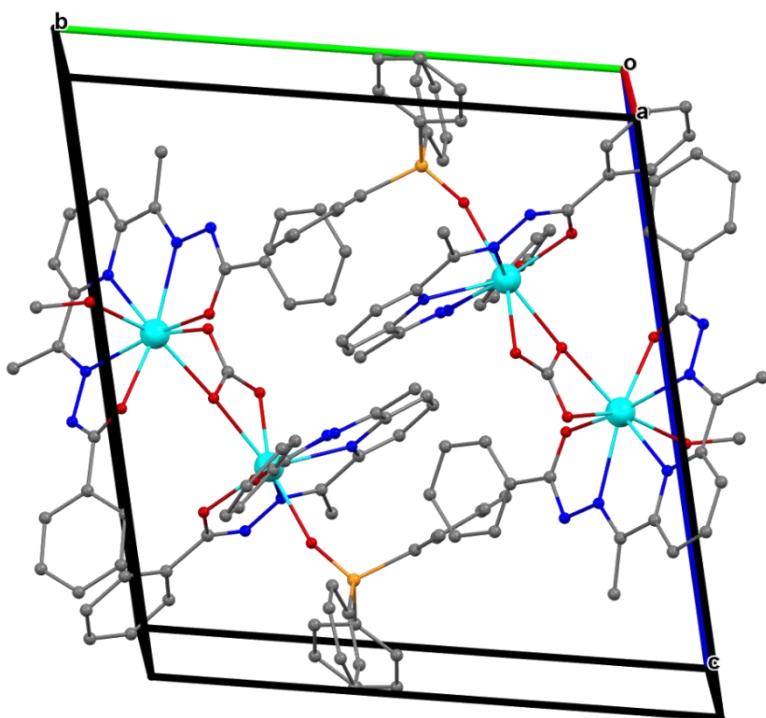
Figure S28: Unit cell contents of **5·Y .** Colour codes: cyan, Y; red, O; blue, N; grey, C; orange ,P
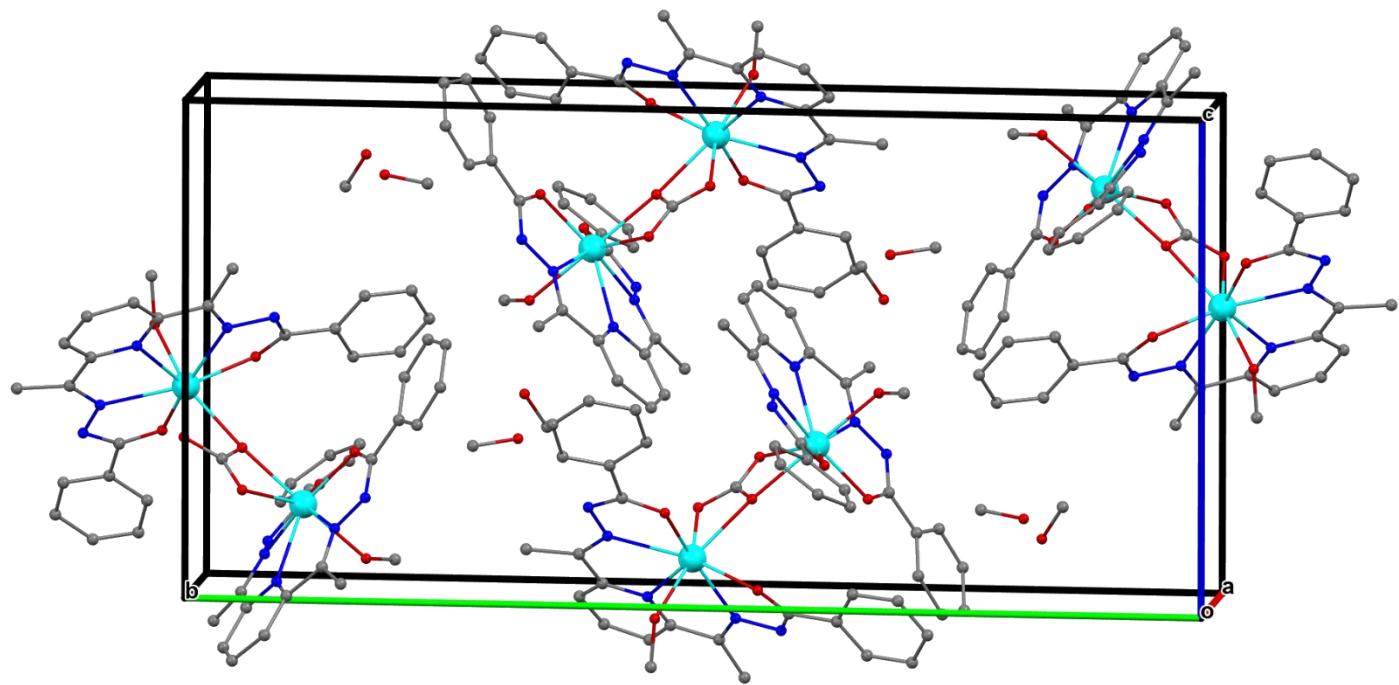
Figure S29: Unit cell contents of **2·Er.** Colour codes: cyan, Er; red, O; blue, N; grey, C
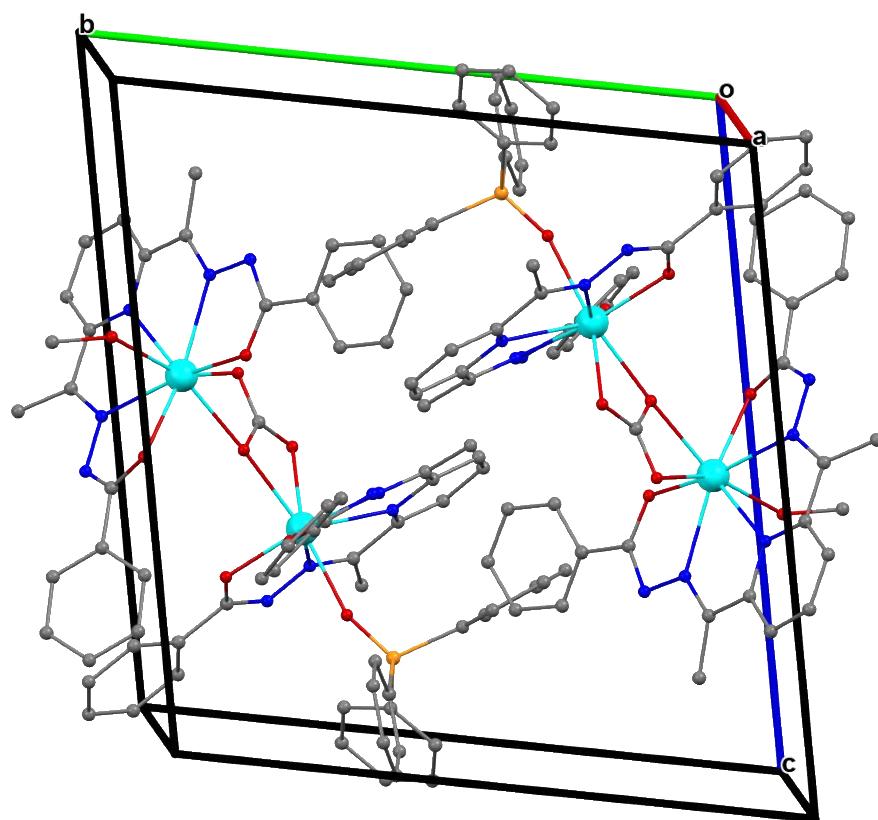
Figure S30: Unit cell contents of **5·Er .** Colour codes: cyan, Er; red, O; blue, N; grey, C; orange, P
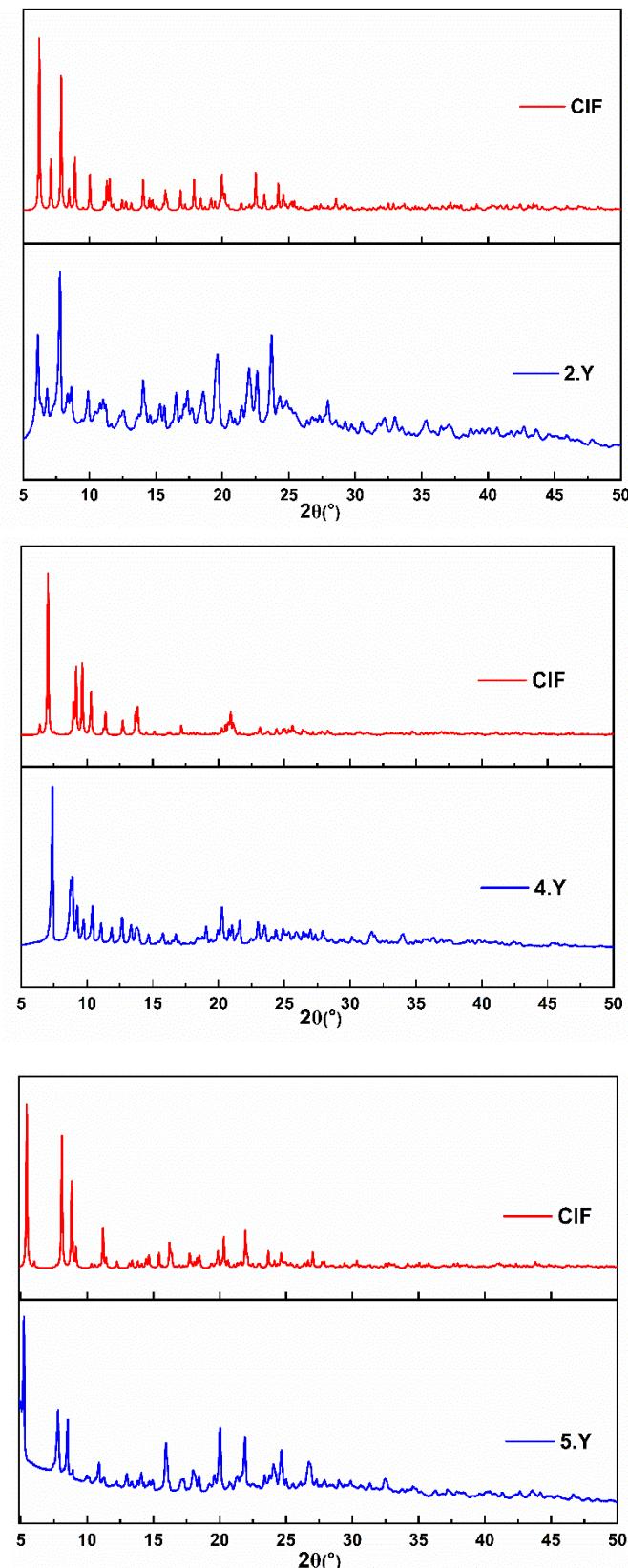
Figure S31: The powder X-ray diffraction patterns of the complexes **2·Y** (*top*), **4·Y** (*middle*), and **5·Y** (*bottom*) recorded at room temperature. Colour codes: experimental, blue; and simulated, red.
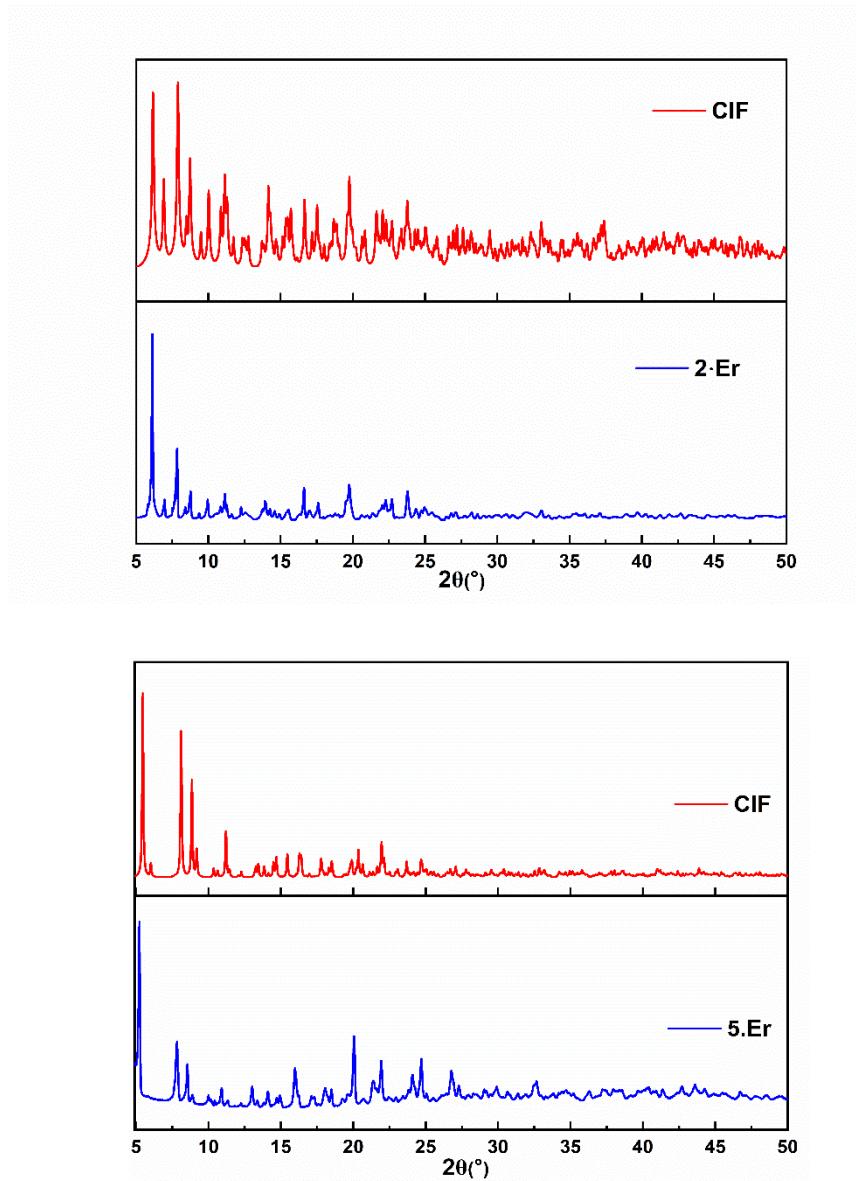
Figure S32: The powder X-ray diffraction patterns of the complexes **2·Er** (*top*), and **5·Er** (*bottom*) recorded at room temperature. Colour codes: experimental, blue; and simulated, red.
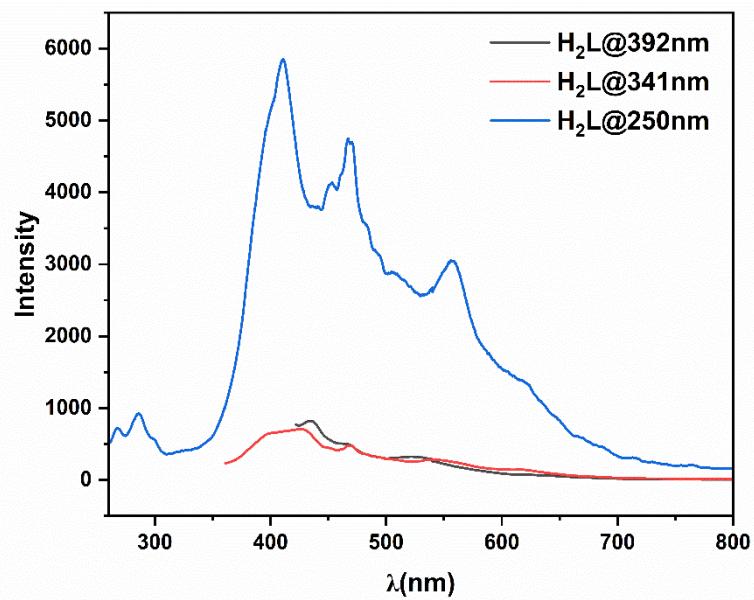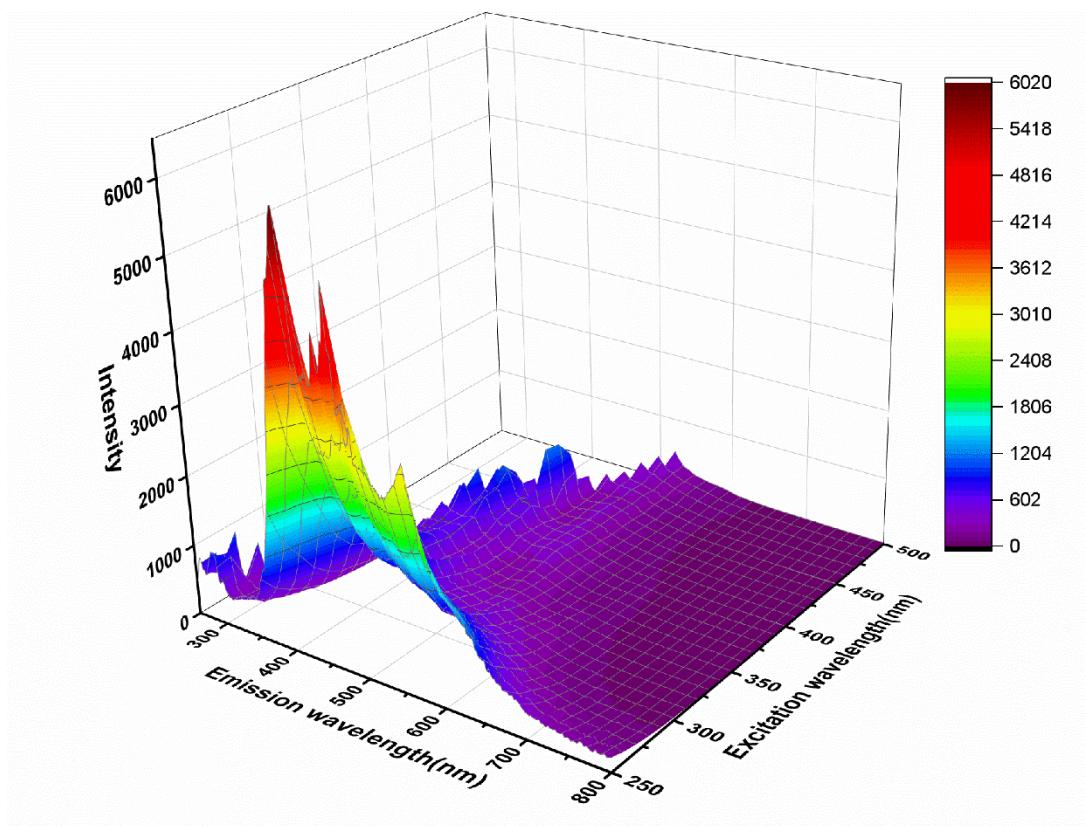
Figure S33: The room temperature photoluminescence excitation spectra of **H₂L** in solid state(top) and emission spectra at mentioned excitation wavelengths(bottom). The spectral characteristics are provided in the main text, and the measurement details are described in the experimental section.
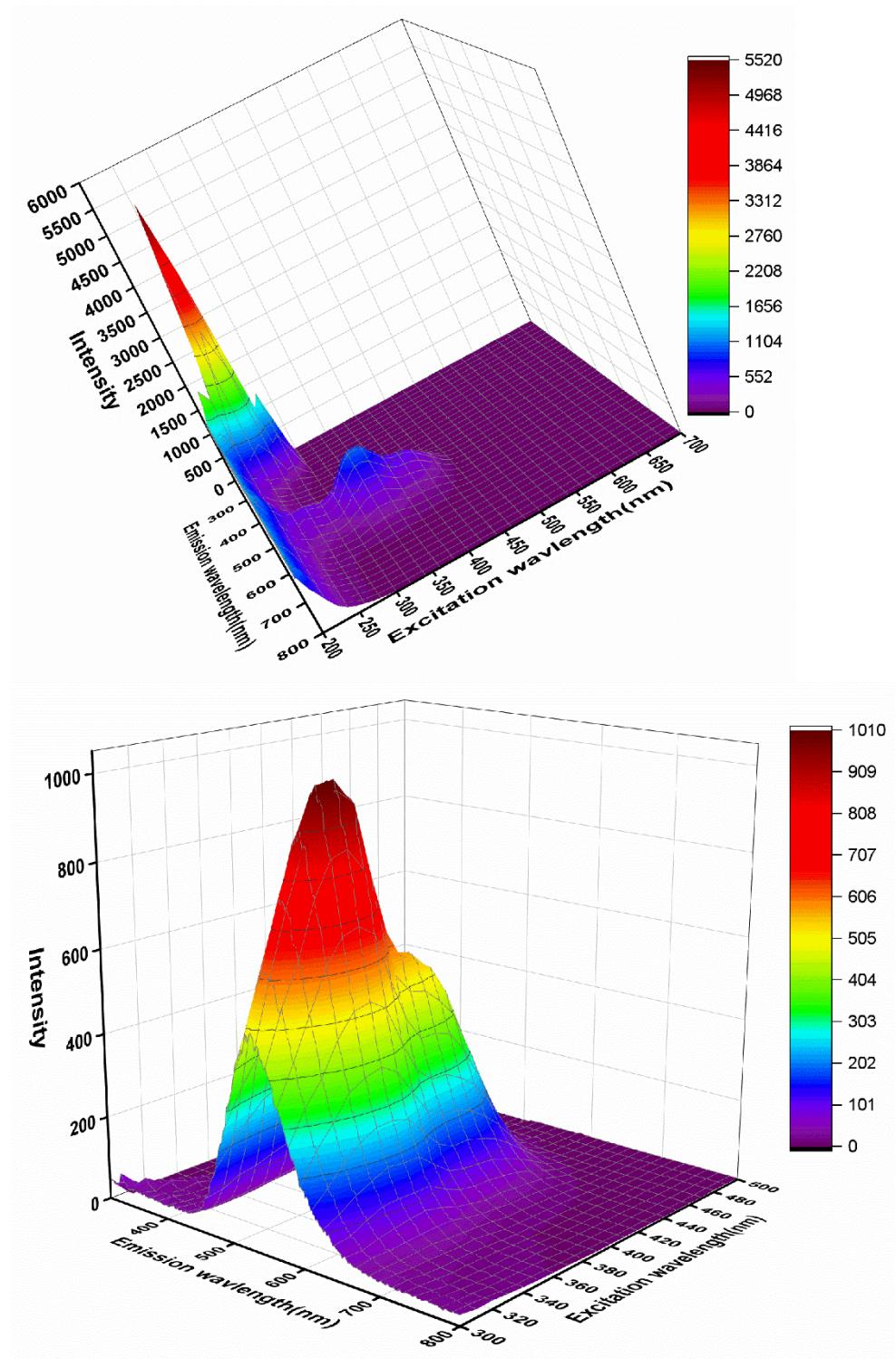
Figure S34: The room temperature photoluminescence excitation spectra of methanolic solutions (10μM) of **2·Y** from 200-700nm(top) and 300-500nm(down). The spectral characteristics are provided in the main text, and the measurement details are described in the experimental section.
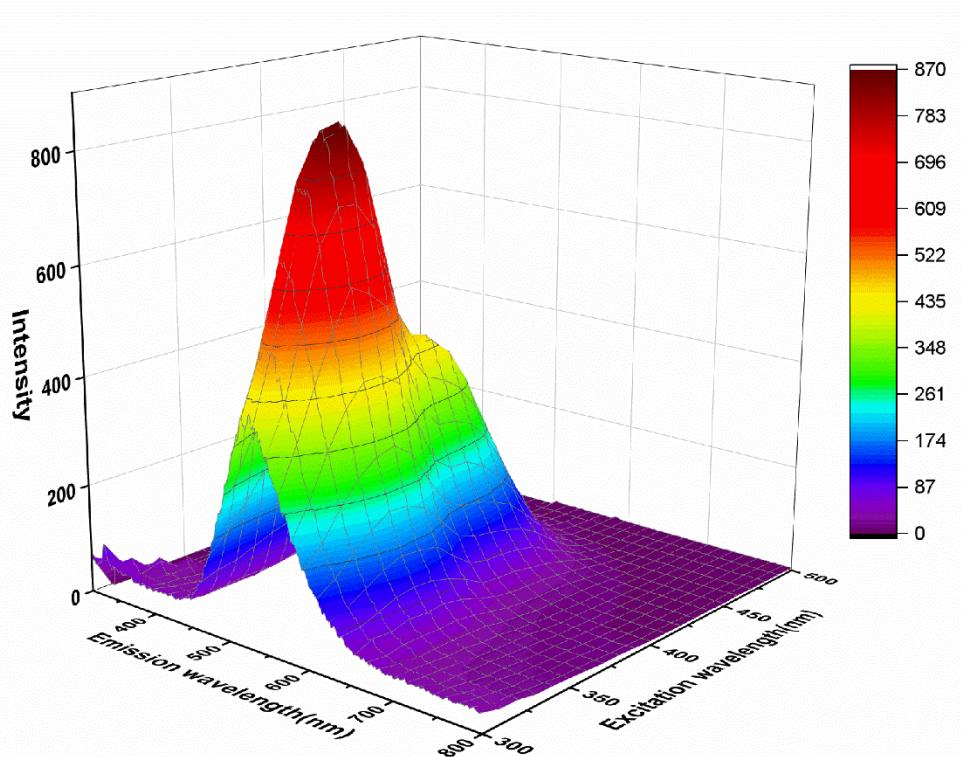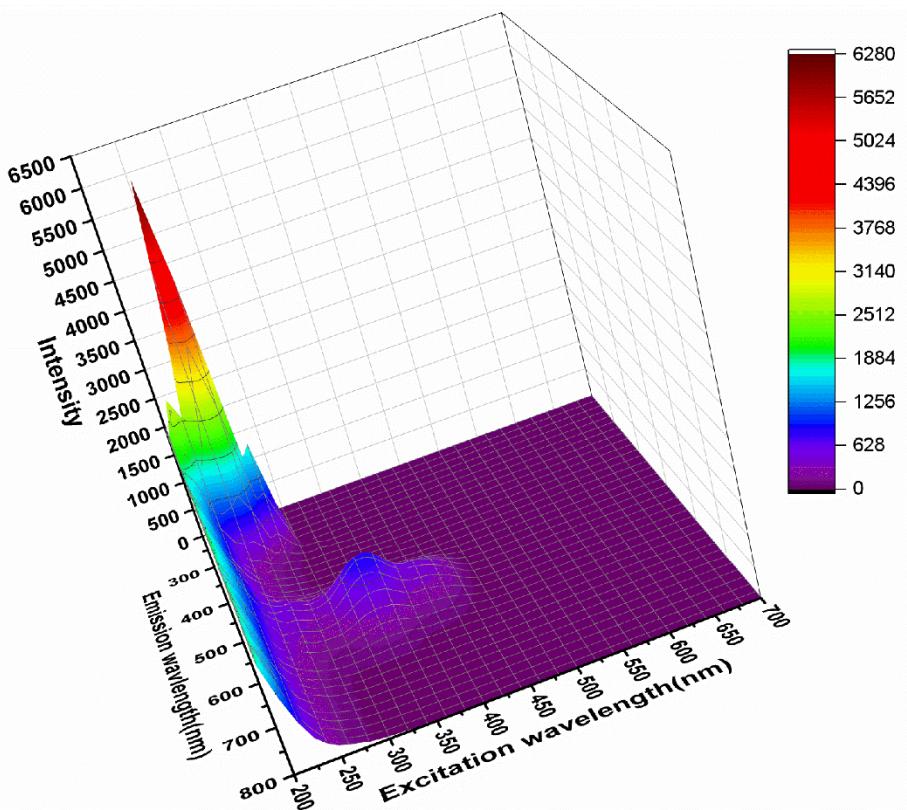
Figure S35: The room temperature photoluminescence excitation spectra of methanolic solutions (10μM) of **5·Y** from 200-700nm(top) and 300-500nm(down). The spectral characteristics are provided in the main text, and the measurement details are described in the experimental section
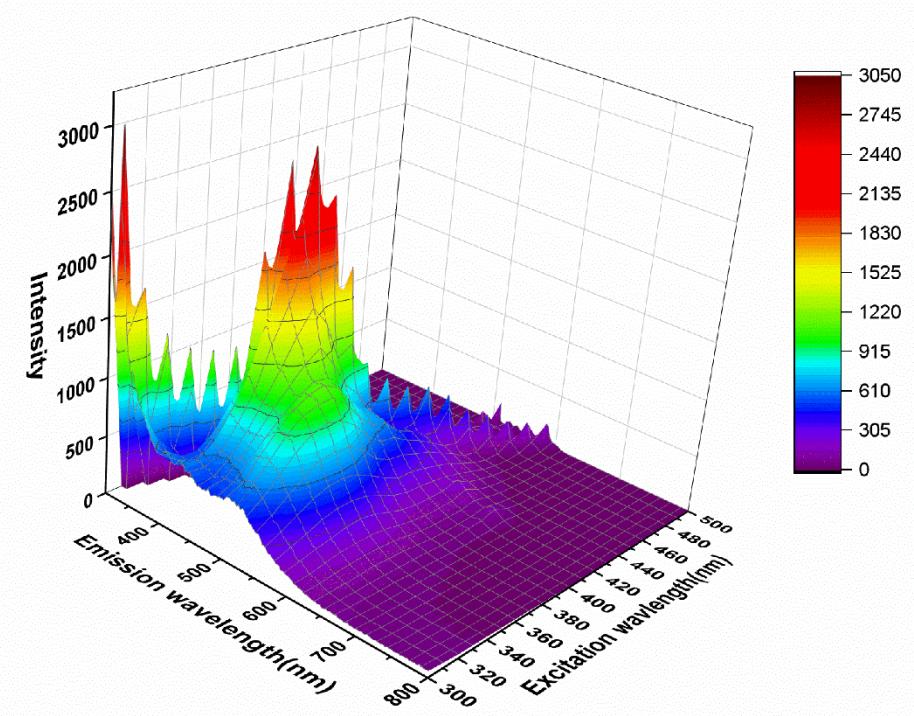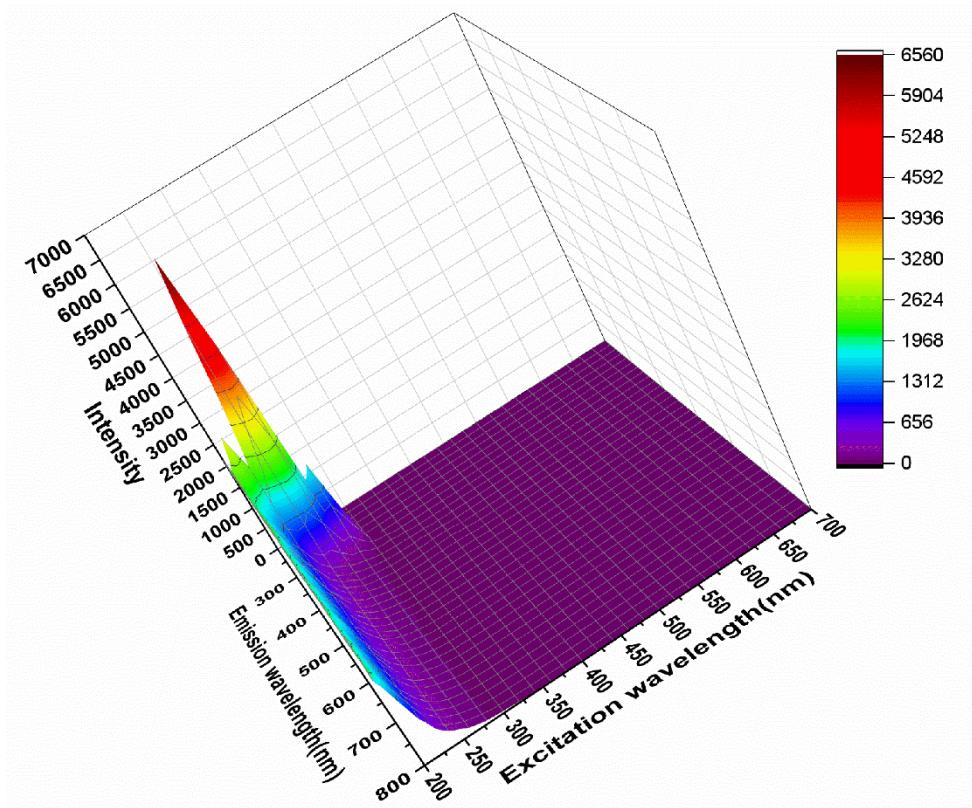
Figure S36: The room temperature photoluminescence excitation spectra of methanolic solutions (10μM) of **2·Er** from 200-700nm(top) and 300-500nm(down). The spectral characteristics are provided in the main text, and the measurement details are described in the experimental section
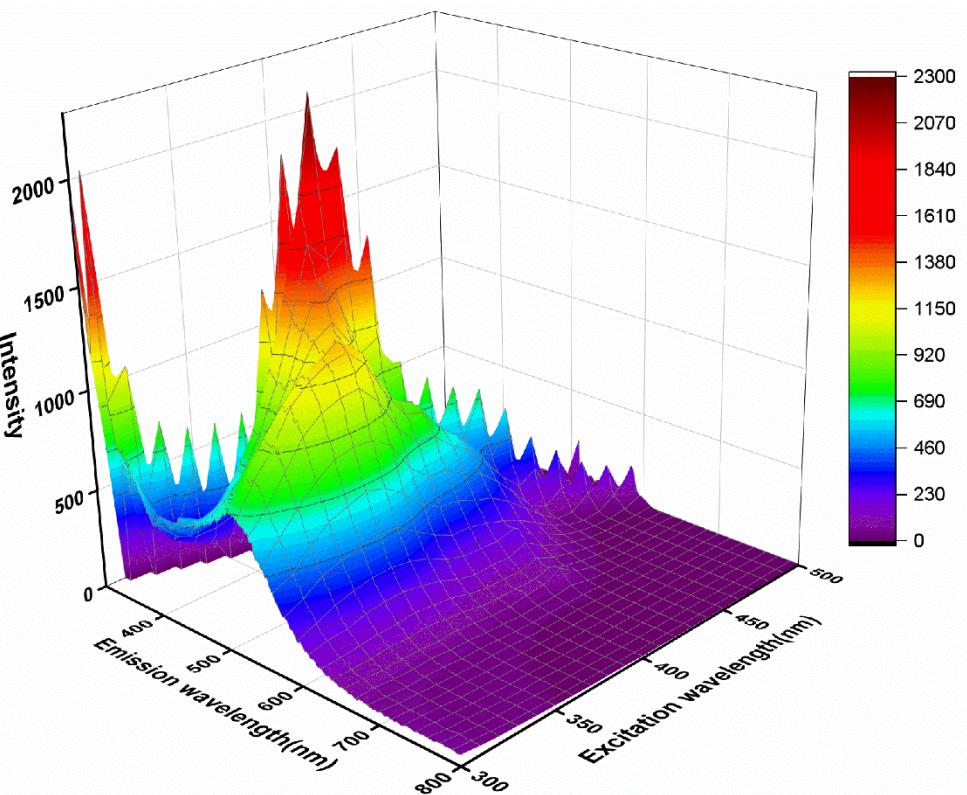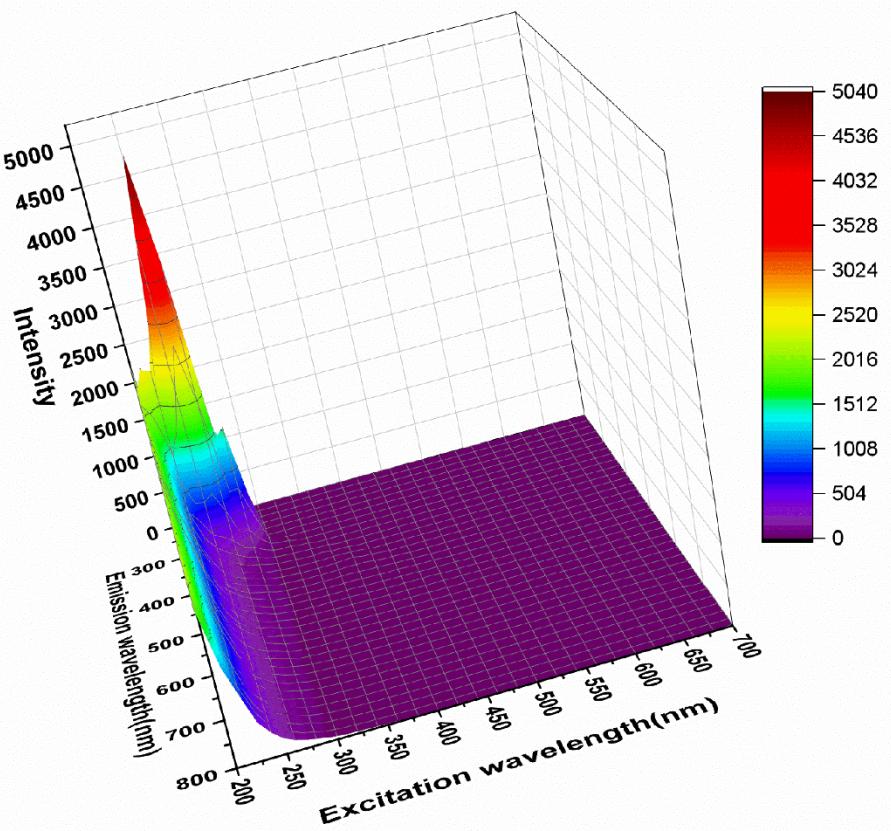
Figure S37: The room temperature photoluminescence excitation spectra of methanolic solutions (10μM) of **5·Er** from 200-700nm(top) and 300-500nm(down). The spectral characteristics are provided in the main text, and the measurement details are described in the experimental section
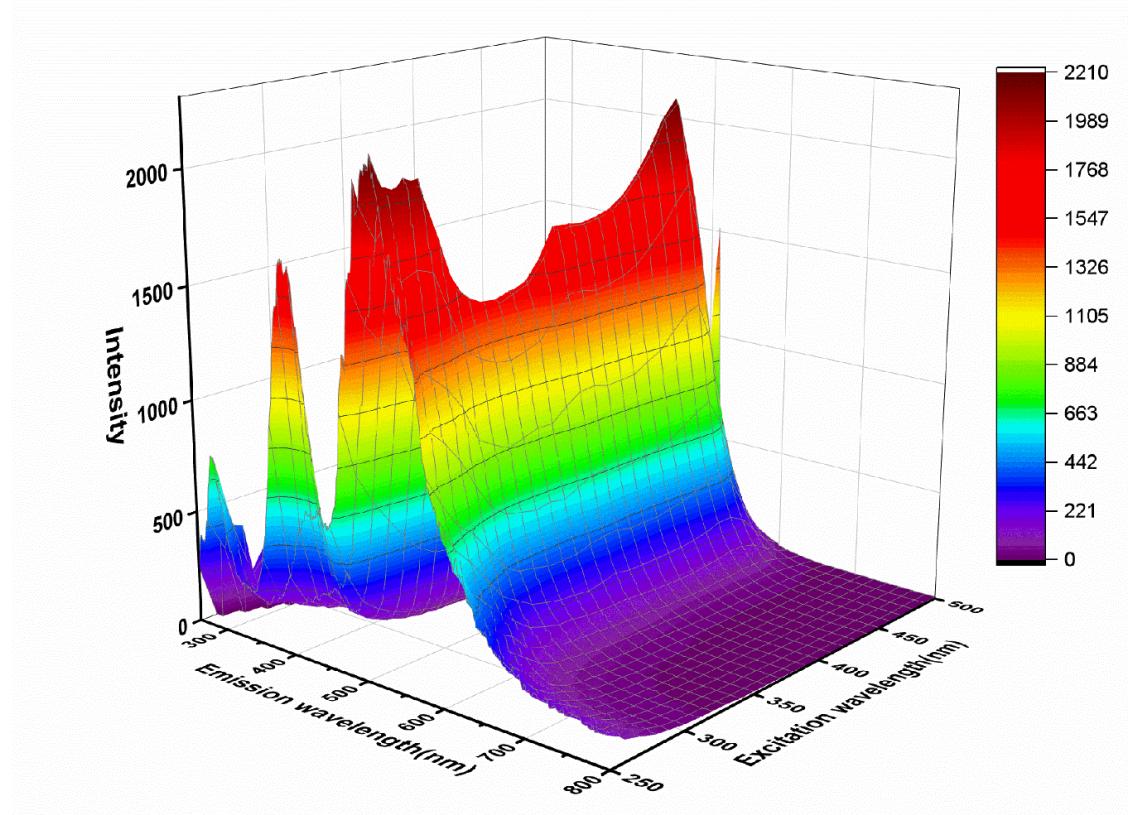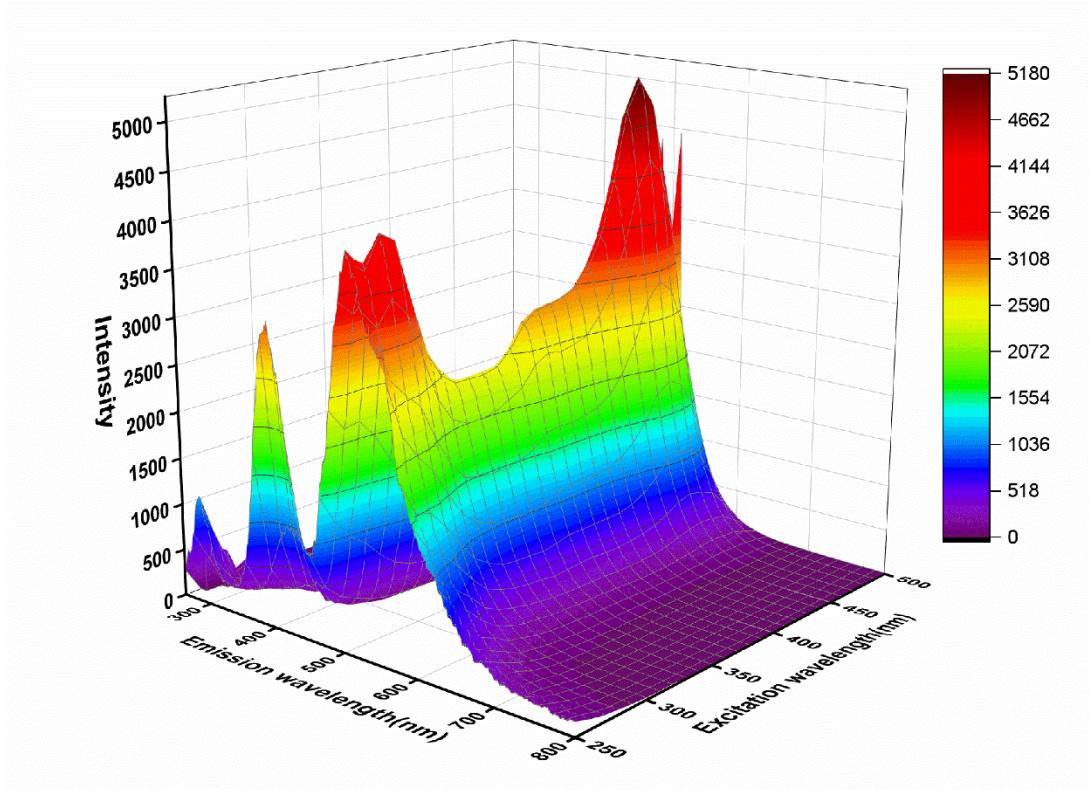
Figure S38: The room temperature photoluminescence excitation spectra of the solid samples **2·Y(top)** and **5·Y(bottom)** from 250 -500 nm. The spectral characteristics are provided in the main text, and the measurement details are described in the experimental section.
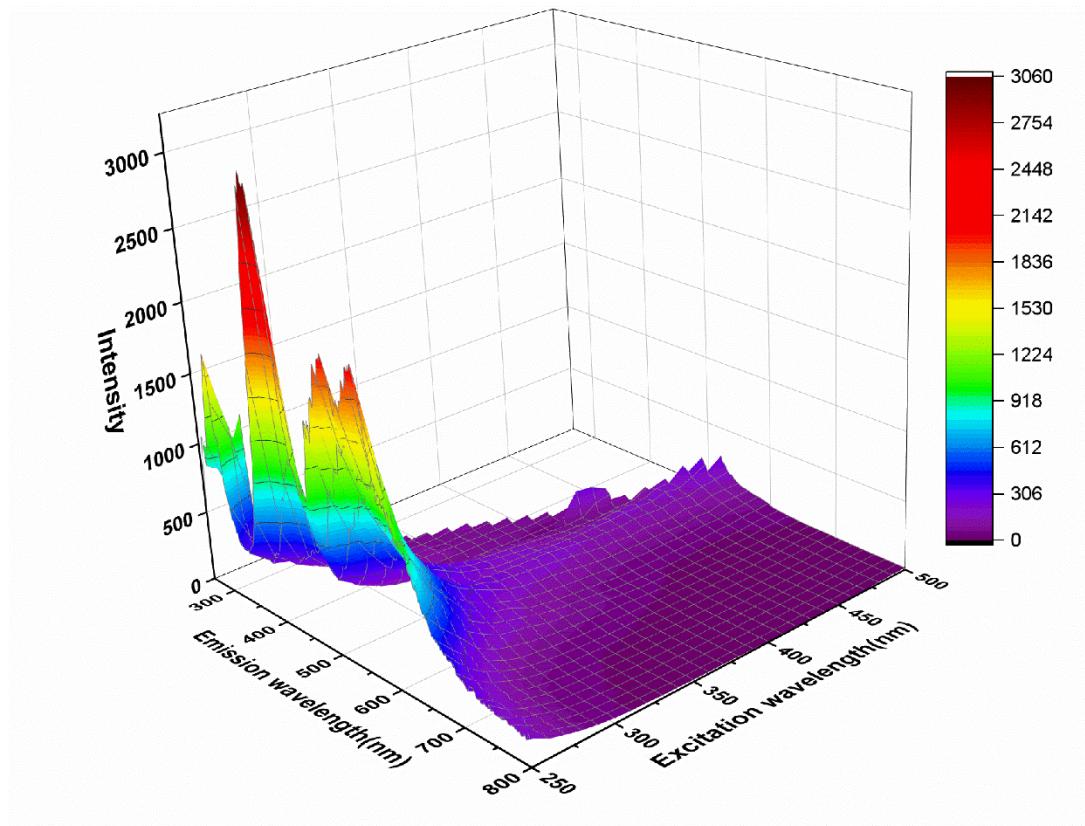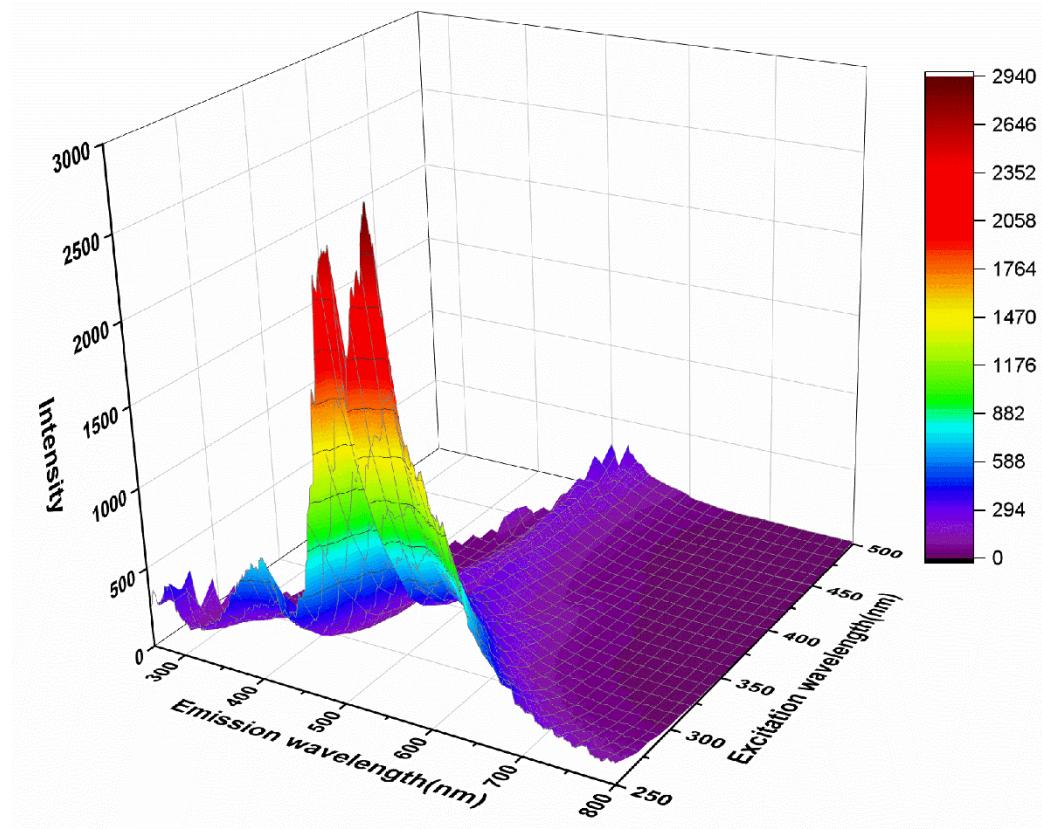
Figure S39: The room temperature photoluminescence excitation spectra of the solid samples **2·Er(top)** and **5·Er(bottom)** from 250 -500 nm. The spectral characteristics are provided in the main text, and the measurement details are described in the experimental section.

Table S5: Selected crystallographic data and refinement parameters for **1·Y, 2·Y, 3·Y, 4·Y, 5·Y and 6·Y**

	1·Y	**2·Y**	**3·Y**
Formula	$C_{50}H_{47}F_3N_{10}O_{12}SY_2$	$C_{51}H_{54}N_{10}O_{11}Y_2$	$C_{50}H_{46}N_{10}O_{11}Y_2$
Mr (g mol^{-1})	1246.85	1160.86	1140.79
crystal system	Monoclinic	Monoclinic	Monoclinic
space group	P 2_1/n	P 2_1/n	P 2_1/n
T (K)	100	100	100
a (Å)	12.9095(3)	12.9182(4)	13.0195(6)
b (Å)	28.744(3)	28.6706(10)	28.4143(15)
c (Å)	15.0415(6)	15.0341(5)	14.6931(7)
α (°)	90	90	90
β (°)	108.009(4)	108.2140(10)	109.381(2)
γ (°)	90	90	90
V (Å^3)	5308.0(9)	5289.2(3)	5127.5(4)
Z	4	4	4
$\rho_{calcd.}$ (g cm^{-3})	1.560	1.458	1.478
μ (mm^{-1})	2.297	2.252	2.321
collected reflns	66465	58883	76086
unique reflns	9469	10866	10527
No. of parameters	689	687	697
Reflns for Refinement	66465	58883	76086
R (I > 3σ(I))^a	0.0677	0.0357	0.0379
wR (I > 3σ(I))^b	0.1959	0.0845	0.0922
GOF on F	1.021	1.015	1.047

	4·Y	**5·Y**	**6·Y**
Formula	$C_{46}H_{39}N_{10}O_4Y$	$C_{66}H_{57}N_{10}O_9PY_2$	$C_{83}H_{68}N_{10}O_9P_2Y_2$
Mr (g mol^{-1})	884.78	1343.00	1589.23
crystal system	Monoclinic	Triclinic	Triclinic
space group	P 2_1/c	P -1	P -1
T (K)	100	150	100
a (Å)	19.6985(10)	12.4890(5)	9.4938(5)
b (Å)	19.6817(10)	15.6025(6)	24.7455(17)
c (Å)	25.6866(13)	17.0019(7)	32.698(2)
α (°)	90	96.001(2)	91.498(2)
β (°)	102.249(2)	103.8000(10)	96.674(2)
γ (°)	90	106.6320(10)	91.932(2)
V (Å^3)	9732.0(9)	3029.1(2)	7621.8(8)
Z	8	2	4
$\rho_{calcd.}$ (g cm^{-3})	1.208	1.472	1.385
μ (mm^{-1})	1.248	2.000	1.622
collected reflns	113555	42238	154166
unique reflns	19972	10634	26652
No. of parameters	1109	801	2022

Reflns for Refinement	113555	42238	154166
$R\ (I > 3\sigma(I))^a$	0.0897	0.0566	0.0711
$wR\ (I > 3\sigma(I))^b$	0.2438	0.1560	0.1899
GOF on F	1.045	1.177	1.027

[a] $R = \Sigma||F_o| - |F_c||/\Sigma|F_o|$, [b] $wR = [\Sigma(w(F_o^2 - F_c^2)^2)/\Sigma\ ([w(F_o^2)^2]^{1/2}$ where $w = 1/(\sigma^2(F_o^2) + (aP)^2 + bP)$ with $P = (2F_c^2 + \max(F_o^2,0))/3$.

Table S6: Selected crystallographic data and refinement parameters for **2·Er and 5·Er**

	2·Er	**5·Er**
Formula	$C_{51}H_{54}Er_2N_{10}O_{11}$	$C_{66}H_{57}Er_2N_{10}O_9P$
Mr (g mol^{-1})	1317.56	1499.70
crystal system	Monoclinic	Triclinic
space group	P 2$_1$/n	P -1
T (K)	100	100
a (Å)	12.9022(3)	12.4588(7)
b (Å)	28.6292(8)	15.5778(8)
c (Å)	15.0283(4)	16.9491(9)
α (°)	90	96.120(2)
β (°)	108.1800(2)	103.752(2)
γ (°)	90	106.503(2)
V (Å^3)	5274.0(2)	3009.5(3)
Z	4	2
$\rho_{calcd.}$ (g cm^{-3})	1.659	1.655
μ (mm^{-1})	3.229	2.864
collected reflns	62454	95368
unique reflns	12082	12324
No. of parameters	689	801
Reflns for Refinement	62454	95368
$R\ (I > 3\sigma(I))^a$	0.0169	0.0171
$wR\ (I > 3\sigma(I))^b$	0.0405	0.0419
GOF on F	1.033	1.073

[a] $R = \Sigma||F_o| - |F_c||/\Sigma|F_o|$, [b] $wR = [\Sigma(w(F_o^2 - F_c^2)^2)/\Sigma\ ([w(F_o^2)^2]^{1/2}$ where $w = 1/(\sigma^2(F_o^2) + (aP)^2 + bP)$ with $P = (2F_c^2 + \max(F_o^2,0))/3$.

Table S7: Selected bond lengths (Å) and bond angles (°) of the complexes **1·Y** ,**2·Y**, **3·Y**, **4·Y, 5·Y, 6·Y, 2·Er, 6·Er**

Complex **1·Y**

Y1 O4	2.318(5)	Y1 O1	2.294(5)	Y1 O3	2.358(5)	Y1 O2	2.305(5)
Y1 O8	2.321(5)	Y1 N3	2.476(5)	Y1 N4	2.444(6)	Y1 N2	2.503(6)
Y2 O7	2.258(5)	Y2 O6	2.293(5)	Y2 O5	2.375(5)	Y2 O3	2.378(5)
Y2 O9	2.396(5)	Y2 N7	2.461(6)	Y2 N9	2.450(6)	Y2 N8	2.454(6)
O7 C34	1.285(8)	O6 C41	1.276(8)	O5 C24	1.256(9)	O4 C24	1.291(8)
O1 C17	1.267(8)	O3 C24	1.311(8)	O2 C10	1.304(8)	N9 N10	1.392(8)
N6 N7	1.384(8)	N5 N4	1.383(8)	N1 N2	1.387(8)		

O1 Y1 N2	63.89(17)	Y1 O3 Y2	172.6(2)	O2 Y1 N4	64.55(17)			
N4 Y1 N3	64.54(18)	N3 Y1 N2	63.71(18)	O7 Y2 N9	65.97(19)			
O6 Y2 N7	64.70(19)	N8 Y2 N7	64.2(2)	N9 Y2 N8	64.42(19)			
C41 N6 N7	108.8(5)	C34 N10 N9	109.4(6)	C17 N1 N2	112.4(5)			
C10 N5 N4	110.3(6)							

Complex **2·Y**

Y1 O4	2.3168(18)	Y1 O1	2.2464(17)	Y1 O3	2.3772(18)	Y1 O2	2.3167(17)
Y1 O8	2.3221(18)	Y1 N3	2.475(2)	Y1 N4	2.450(2)	Y1 N2	2.484(2)
Y2 O7	2.2539(18)	Y2 O6	2.2793(18)	Y2 O5	2.3620(17)	Y2 O3	2.3679(18)
Y2 O9	2.4056(18)	Y2 N7	2.452(2)	Y2 N9	2.448(2)	Y2 N8	2.453(2)
O7 C34	1.286(3)	O6 C41	1.280(3)	O5 C24	1.260(3)	O4 C24	1.275(3)
O1 C17	1.283(3)	O3 C24	1.319(3)	O2 C10	1.294(3)	N9 N10	1.384(3)
N7 N6	1.394(3)	N4 N5	1.393(3)	N1 N2	1.397(3)		

O1 Y1 N2	64.30(6)	Y2 O3 Y1	174.80(9)	O2 Y1 N4	64.23(6)
N4 Y1 N3	64.23(7)	N3 Y1 N2	64.14(7)	O7 Y2 N9	65.71(7)
O6 Y2 N7	65.01(7)	N7 Y2 N8	63.92(7)	N9 Y2 N8	64.57(7)
C10 N5 N4	109.6(2)	C17 N1 N2	108.5(2)	C41 N6 N7	108.4(2)
C34 N10 N9	109.1(2)				

Complex **3·Y**

Y1 O4	2.348(2)	Y1 O1	2.278(2)	Y1 O3	2.367(2)	Y1 O2	2.295(2)
Y1 O8	2.385(2)	Y1 N3	2.447(3)	Y1 N4	2.431(3)	Y1 N2	2.448(2)
Y2 O7	2.279(2)	Y2 O6	2.306(2)	Y2 O5	2.321(2)	Y2 O3	2.383(2)
Y2 O9	2.374(2)	Y2 N7	2.419(2)	Y2 N9	2.458(2)	Y2 N8	2.450(2)
O7 C34	1.292(4)	O6 C41	1.289(3)	O5 C24	1.272(4)	O4 C24	1.262(3)
O1 C17	1.295(4)	O3 C24	1.315(3)	O2 C10	1.277(4)	N9 N10	1.393(3)
N6 N7	1.388(3)	N4 N5	1.390(4)	N1 N2	1.391(3)		

O1 Y1 N2	65.37(8)	Y1 O3 Y2	175.92(10)	O2 Y1 N4	65.24(8)
N4 Y1 N3	64.37(9)	N3 Y1 N2	64.53(9)	O7 Y2 N9	64.78(8)
O6 Y2 N7	65.10(8)	N7 Y2 N8	64.98(8)	N8 Y2 N9	64.62(8)
C10 N5 N4	108.8(3)	C17 N1 N2	109.7(2)	C41 N6 N7	109.5(2)
C34 N10 N9	109.2(2)				

Complex 4·Y

O2	C10	1.276(8)	N4	N5	1.384(7)	Y1	O2	2.451(4)	Y1 N4	2.514(5)
Y1	N3	2.638(5)	N1	N2	1.380(7)	Y1	N2	2.553(5)	O1 C17	1.280(7)
O4	C33	1.259(8)	N10	N9	1.400(7)	Y1	O4	2.505(4)	Y1 N9	2.554(5)
Y1	N8	2.618(5)	Y1	O1	2.377(4)	Y1	N7	2.494(5)	N6 N7	1.383(8)
O3	C40	1.265(7)	Y1	O3	2.333(4)	O7	C56	1.261(7)	Y2 O7	2.390(4)
N20	N21	1.418(7)	Y2	N20	2.491(5)	Y2	N19	2.646(5)	Y2 N17	2.567(5)
N16	N17	1.392(7)	O8	C63	1.227(7)	Y2	O8	2.506(4)	O5 C79	1.273(7)

O7 Y2 N20	62.28(16)	O8 Y2 N17	60.41(15)	N20 Y2 N19	60.73(17)
N17 Y2 N19	59.51(16)	O5 Y2 N12	61.16(15)	N12 Y2 N13	60.64(15)
N14 Y2 N13	61.68(15)	O6 Y2 N14	62.06(15)	O4 Y1 N9	60.36(16)
N9 Y1 N8	60.31(17)	N7 Y1 N8	62.05	O3 Y1 N7	62.51(16)
O2 Y1 N4	60.75(17)	N4 Y1 N3	61.16(16)	N2 Y1 N3	60.52(15)
O1 Y1 N2	61.11(15)	C17 N1 N2	108.5(5)	C10 N5 N4	107.5(5)
C40 N6 N7	106.9(5)	C33 N10 N9	113.9(5)	C86 N15 N14	107.4(5)
C79 N11 N12	108.0(5)	C56 N21 N20	107.8(5)	C63 N16 N17	113.7(5)

Complex 5·Y

Y1	O4	2.314(4)	Y1	O1	2.248(4)	Y1	O3	2.386(4)	Y1 O2	2.319(4)
Y1	O8	2.342(4)	Y1	N3	2.484(5)	Y1	N4	2.458(4)	Y1 N2	2.483(5)
Y2	O7	2.265(4)	Y2	O6	2.301(4)	Y2	O5	2.376(4)	Y2 O3	2.389(4)
Y2	O9	2.323(4)	Y2	N7	2.462(5)	Y2	N9	2.468(5)	Y2 N8	2.486(5)
O7	C34	1.289(7)	O6	C41	1.271(7)	O5	C24	1.263(7)	O4 C24	1.265(7)
O1	C17	1.282(7)	O3	C24	1.321(6)	O2	C10	1.293(7)	N10 N9	1.389(6)
N6	N7	1.388(7)	N4	N5	1.398(6)	N1	N2	1.391(6)		

O1 Y1 N2	64.24(14)	Y1 O3 Y2	175.53(19)	O2 Y1 N4	63.80(14)
N4 Y1 N3	64.06(15)	N2 Y1 N3	63.94(15)	O7 Y2 N9	65.03(15)
O6 Y2 N7	64.77(14)	N7 Y2 N8	64.00(15)	N9 Y2 N8	63.92(15)
C10 N5 N4	108.7(4)	C17 N1 N2	107.9(4)	C34 N10 N9	109.5(5)
C41 N6 N7	108.7(4)				

Complex 6·Y

Y4 O15	2.371(4)	Y4 O16	2.249(4)	Y4 O14	2.228(5)	Y4 O18	2.300(5)
Y4 O12	2.390(5)	Y4 N19	2.426(5)	Y4 N18	2.443(5)	Y4 N17	2.438(5)
Y3 O17	2.315(5)	Y3 O10	2.339(4)	Y3 O12	2.381(5)	Y3 O13	2.263(5)
Y3 N13	2.443(6)	Y3 O11	2.294(5)	Y3 N12	2.451(6)	Y3 N14	2.482(7)
Y1 O8	2.280(4)	Y1 O1	2.269(4)	Y1 O3	2.374(4)	Y1 O2	2.379(4)
Y1 N2	2.459(4)	Y1 O4	2.234(5)	Y1 N4	2.447(5)	Y1 N3	2.453(4)
Y2 O3	2.347(4)	Y2 O6	2.280(4)	Y2 O9	2.305(4)	Y2 O7	2.303(5)
Y2 O5	2.282(5)	Y2 O7	2.303(5)	Y2 N8	2.453(5)	Y2 N9	2.426(5)
O15 C124	1.271(7)	O16 C117	1.295(7)	O14 C107	1.292(8)	O12 C107	1.296(7)
O1 C17	1.290(6)	O10 C100	1.286(7)	O3 C47	1.267(7)	O2 C10	1.285(7)
N19 N20	1.399(8)	C107 O13	1.248(8)	N11 N12	1.390(8)	N2 N1	1.392(6)
N16 N17	1.389(7)	N7 N6	1.391(7)	N5 N4	1.392(6)	O11 C93	1.286(9)
N9 N10	1.377(7)	O6 C40	1.272(7)	O7 C33	1.288(9)	O4 C47	1.288(7)

O3	C47		1.267(7)	N14	N15		1.387(10)		

O1	Y1	N2	65.59(14)	Y2	O3	Y1	176.3(2)	O2	Y1	N4	63.76(14)
N4	Y1	N3	64.73(15)	O7	Y2	N9	64.88(18)	O6	Y2	N7	63.82(15)
N8	Y2	N7	65.06(17)	N9	Y2	N8	65.37(18	N3	Y1	N2	64.58(15)
O10	Y3	N12	63.89(16)	N13	Y3	N12	64.3(2)	N13	Y3	N14	65.4(3)
O11	Y3	N14	63.4(2)	Y3	O12	Y4	168.1(3)	O15	Y4	N17	63.80(16)
N17	Y4	N18	64.61(18)	N19	Y4	N18	65.5(2)	O16	Y4	N19	66.26(17)
C10	N5	N4	109.1(4)	C17	N1	N2	109.5(4)	C33	N10	N9	110.3(6)
C40	N6	N7	108.5(5)	C117	N20	N19	109.5(5)	C124	N16	N17	108.0(5)
C93	N15	N14	109.0(7)	C100	N11	N12	109.3(5)				

Complex 2·Er

Er1	O4	2.3536(13)	Er1	O1	2.2498(13)	Er1	O3	2.3615(13)	Er1	O2	2.2776(13)
Er1	O8	2.3994(13)	Er1	N3	2.4320(16)	Er1	N4	2.4418(16)	Er1	N2	2.4313(16)
Er2	O7	2.2445(12)	Er2	O6	2.3089(13)	Er2	O5	2.3080(13)	Er2	O3	2.3742(13)
Er2	O9	2.3130(13)	Er2	N7	2.4341(15)	Er2	N9	2.4747(16)	Er2	N8	2.4610(15)
O7	C34	1.278(2)	O6	C41	1.298(2)	O5	C24	1.275(2)	O4	C24	1.265(2)
O1	C17	1.289(2)	O3	C24	1.315(2)	O2	C10	1.280(2)	N10	N9	1.395(2)
N6	N7	1.392(2)	N4	N5	1.387(2)	N1	N2	1.387(2)			

O1	Er1	N2	65.98(5)	Er1	O3	Er2	175.06(6)	O2	Er1	N4	65.22(5)
N3	Er1	N4	64.32(5))	N2	Er1	N3	65.00(5)	O7	Er2	N9	64.62(5)
O6	Er2	N7	64.56(5)	N7	Er2	N8	64.54(5)	N8	Er2	N9	64.42(5)
C10	N5	N4	108.29(16)	C17	N1	N2	109.22(15)	C34	N10	N9	108.57(15)
C41	N6	N7	109.42(15)								

Complex 5·Er

Er1	O4	2.3115(13)	Er1	O1	2.3050(13)	Er1	O3	2.3833(13)	Er1	O2	2.2451(13)
Er1	O8	2.3341(13)	Er1	N3	2.4674(16)	Er1	N4	2.4699(16)	Er1	N2	2.4442(15)
Er2	O7	2.2939(13)	Er2	O6	2.2578(13)	Er2	O5	2.3660(14)	Er2	O3	2.3852(13)
Er2	O9	2.3146(14)	Er2	N7	2.4482(16)	Er2	N9	2.4451(15)	Er2	N8	2.4607(15)
O7	C34	1.275(2)	O6	C41	1.283(2)	O5	C24	1.268(2)	O4	C24	1.274(2)
O1	C17	1.297(2)	O3	C24	1.316(2)	O2	C10	1.287(2)	N9	N10	1.391(2)
N7	N6	1.390(2)	N5	N4	1.394(2)	N1	N2	1.389(2)			

O1	Er1	N2	64.28(5)	Er1	O3	Er2	176.08(6)	O2	Er1	N4	64.82(5)
N3	Er1	N4	64.09(5)	N2	Er1	N3	64.40(5)	O7	Er2	N9	65.09(5)
O6	Er2	N7	65.25(5)	N7	Er2	N8	64.39(5)	N9	Er2	N8	64.22(5)
C10	N5	N4	108.71(15)	C17	N1	N2	109.37(15)	C34	N10	N9	108.68(15)
C41	N6	N7	108.64(15)								

Table S8: The outputs from the *Continuous Shape Measures* (CShM's) analyses employing the SHAPE program based on the Pinsky-Avnir algorithm for the calculation of continuous shape measures for the **1·Y-6·Y, 2·Er and 5·Er** octacoordinated fragments around the Ln centers in the complexes with highlighted closest geometry (minimal distortion paths values) for each metal center.

Complex **1·Y**

Metal Centre Polyhedron*	Y1	Y2
OP-8	34.420	32.442
HPY-8	23.505	22.509
HBPY-8	11.352	16.356
CU-8	9.252	14.007
SAPR-8	4.411	4.777
TDD-8	3.928	2.816
JGBF-8	9.442	12.311
JETBPY-8	24.811	26.112
JBTPR-8	4.380	3.968
BTPR-8	3.698	3.314
JSD-8	5.401	4.772
TT-8	10.098	14.535
ETBPY-8	22.266	23.011

Complex **2·Y**

Metal Centre Polyhedron*	Y1	Y2
OP-8	34.078	32.213
HPY-8	23.679	22.488
HBPY-8	11.699	16.804
CU-8	9.670	13.819
SAPR-8	4.381	4.686
TDD-8	4.026	2.832
JGBF-8	9.351	12.813
JETBPY-8	25.036	26.378
JBTPR-8	4.285	3.952
BTPR-8	3.604	3.293
JSD-8	5.069	4.826
TT-8	10.500	14.345
ETBPY-8	22.513	23.295

Complex **3·Y**

Metal Centre Polyhedron*	Y1	Y2
OP-8	33.109	34.588
HPY-8	21.992	23.439
HBPY-8	16.615	12.701
CU-8	14.019	10.425
SAPR-8	5.232	4.452
TDD-8	**2.919**	3.702
JGBF-8	12.501	10.061
JETBPY-8	25.542	25.104
JBTPR-8	4.231	4.113
BTPR-8	3.630	**3.299**
JSD-8	4.702	4.985
TT-8	14.605	11.237
ETBPY-8	22.524	22.350

Complex **5·Y**

Metal Centre Polyhedron*	Y1	Y2
OP-8	31.751	33.723
HPY-8	23.206	23.116
HBPY-8	11.990	14.436
CU-8	10.343	12.630
SAPR-8	4.930	5.299
TDD-8	**3.634**	**3.274**
JGBF-8	9.413	10.507
JETBPY-8	25.055	25.041
JBTPR-8	4.482	4.678
BTPR-8	3.795	3.974
JSD-8	4.618	4.766
TT-8	11.111	13.336
ETBPY-8	22.295	22.084

Complex **6·Y**

Metal Centre Polyhedron*	Y1	Y2	Y3	Y4
OP-8	32.430	32.915	32.297	32.385
HPY-8	22.976	22.287	22.716	22.518
HBPY-8	12.230	10.645	11.518	13.441
CU-8	11.011	9.357	11.005	12.265
SAPR-8	4.814	5.275	5.486	5.120
TDD-8	**3.156**	3.848	**3.668**	**2.887**
JGBF-8	9.687	9.772	8.906	10.480
JETBPY-8	23.878	24.744	23.344	24.346

JBTPR-8	4.703	4.365	5.062	4.156
BTPR-8	4.208	**3.599**	4.602	3.711
JSD-8	4.433	5.698	4.833	4.386
TT-8	11.523	10.036	11.672	12.699
ETBPY-8	21.242	22.175	20.197	21.515

Complex **2·Er**

Metal Centre Polyhedron*	Er1	Er2
OP-8	32.167	34.198
HPY-8	22.494	23.677
HBPY-8	16.869	11.820
CU-8	13.580	9.779
SAPR-8	4.559	4.304
TDD-8	**2.722**	3.901
JGBF-8	12.928	9.411
JETBPY-8	26.610	25.184
JBTPR-8	3.865	4.172
BTPR-8	3.201	**3.490**
JSD-8	4.772	4.964
TT-8	14.129	10.607
ETBPY-8	23.520	22.665

Complex **5·Er**

Metal Centre Polyhedron*	Er1	Er2
OP-8	31.913	33.768
HPY-8	23.129	23.248
HBPY-8	12.155	14.483
CU-8	10.480	12.646
SAPR-8	4.829	5.180
TDD-8	**3.460**	**3.154**
JGBF-8	9.537	10.571
JETBPY-8	25.292	25.248
JBTPR-8	4.348	4.576
BTPR-8	3.629	3.853
JSD-8	4.501	4.691
TT-8	11.254	13.367
ETBPY-8	22.509	22.281

* OP-8: Octagon (D8h); HPY-8: Heptagonal pyramid (C7v); HBPY-8: Hexagonal bipyramid (D6h); CU-8: Cube (Oh); SAPR-8: Square antiprism (D4d); TDD-8: Triangular dodecahedron (D2d); JGBF-8: Johnson gyrobifastigium J26 (D2d); JETBPY-8: Johnson elongated triangular bipyramid J14 (D3h); JBTPR-8: Biaugmented trigonal prism J50 (C2v); BTPR-8: Biaugmented trigonal prism (C2v); JSD-8: Snub diphenoid J84 (D2d); TT-8: Triakis tetrahedron (Td); ETBPY-8: Elongated trigonal bipyramid (D3h).

Ref:
1. Lorenzini, C., Pelizzi, C., Pelizzi, G., & Predieri, G., Journal of the Chemical Society, Dalton Transactions **1983**, 4, 721-727.
2. Dubovan, L., Pollnitz, A., Silvestru, C. Eur. J. Inorg. Chem. **2016**, 10, 1521−1527.
3. International Tables for Crystallography.
4. M. Décultot, A. Ledoux, M.-C. Fournier-Salaün, L. Estel, *J. Chem. Thermodyn.* **2019**, *138*, 67-77.